Summer 2017

Imaging in karst terrain using the electrical resistivity and multichannel analyses of surface wave methods

Ragab W. Jaafar

IMAGING IN KARST TERRAIN USING THE ELECTRICAL RESISTIVITY AND MULTICHANNEL ANALYSES OF SURFACE WAVE METHODS

by

RAGAB W JAAFAR

A THESIS

Presented to the Faculty of the Graduate School of the

MISSOURI UNIVERSITY OF SCIENCE AND TECHNOLOGY

In Partial Fulfillment of the Requirements for the Degree

MASTER OF SCIENCE

IN

GEOLOGICAL ENGINEERING

2017

Approved by

Neil L. Anderson, Advisor

Evgeniy Torgashov

Kelly Liu

ABSTRACT

Electrical resistivity tomography and multi-channel analyses of surface waves data were acquired at a study area in Phelps County in the south-central part of Missouri. The objectives of the investigation were fourfold: 1) to image the subsurface in the study area to a depth of 70 feet; 2) to compare the ERT images generated using both the dipole-dipole and Wenner-Schlumberger arrays; and 3) to assess how variations in the MASW array configuration affected MASW data quality; and 4) to compare the ERT-estimated depth to top-of-rock and the MASW-generated depth to top-of-rock.

The subsurface in the study area was imaged to a depth of 70 feet using the ERT tool. Soils were categorized as either dry, moist or moist and clayey. Limestone bedrock was also imaged and categorized as weathered or intact. The top-of-rock, as per the ERT interpretations, was consistent with the MASW-estimated depths to top-of-rock and correlated well with the 70 ohm-m contour value.

Based on the comparative analyses of the dipole-dipole array ERT data, the Wenner-Schlumberger array ERT data and MASW 1-D shear-wave data, it is concluded that the Wenner-Schlumberger array ERT data are slightly more consistent with the MASW data in terms of estimated depth to top-of-rock and dip direction of subsurface layers. However, the dipole-dipole array ERT data appear to better image limestone bedrock (in terms of lateral resolution). Based on the analyses of the MASW data, it is concluded that better results were obtained using a 2.5-foot geophone spacing (as opposed to a 5-foot spacing), probably because depth to top-of-rock varies significantly in places in the study area.

ACKNOWLEDGMENTS

I would like to express my sincere gratitude to my advisor Dr. Neil Anderson for his endless patience, motivation, and immense knowledge during the period of this research. I would also like to thank my committee members Dr. Kelly Liu and Dr. Evgeniy Torgashov for their support and insightful comments.

My grateful thanks extend to all staff members of the Department of Geological Engineering who made my stay at the university fruitful and enjoyable. I would like to thank S&T graduate student Adel Elkrry and Stanley Nwokebuihe for providing help in the project.

Specifically, I would like to thank Mr. Kenneth and his family for giving us an area in their farm for conducting this research.

Finally, my sincere appreciations must go to my parents, my wife, my brother, my sisters and my beloved one my daughter Bodoor for their support and incredible patience throughout my study.

TABLE OF CONTENTS

LIST OF ILLUSTRATIONS

LIST OF TABLES

1. INTRODUCTION

1.1. BACKGROUND

Determining the geotechnical properties and geological structures of the shallow subsurface in karst terrains, for instance the stiffens of the top soil layers and the depth of bedrock, is crucial in different civil and environmental engineering projects. Geophysical methods such as microgravity, ground penetration radar, seismic refraction, multichannel analysis of surface waves (MASW), and electrical resistivity tomography (ERT) are able to image the subsurface features remotely and distinguish physical properties of subsurface materials by creating measurements at the ground without drilling. According to Chalikakis et al. (2011), geophysical explorations in karst areas have expanded swiftly because of technological advancements, cost-effectiveness, straightforward field approaches and rapid inversion and interpretation of data. Additionally, since the geophysical methods are applicable when investigating and solving an assortment of environmental, engineering, and archaeological issues, they have become widely utilized in delineation of subsurface cavities and deserted tunnels (Chalikakis et al., 2011).

Nevertheless, a karst territory remains a complex environment for all geophysical investigation; determining the most appropriate geophysical techniques is not always apparent, because of unpredictably changeable subsurface features and the limitation of using various geophysical methods.

Burger et al. (2006) explain that the goals of certain subsurface investigation usually cannot be achieved by using only one geophysical technique. This is because of the limitations and ambiguities of using one method such as resolution, noise, and the absence of adequate contrast in physical properties that can restrict the geophysical

methods in various cases (Burger et al., 2006). Surface wave methods are often utilized to estimate shear wave velocity profile of subsurface materials, but the field measurements of this wave frequently consist of undesirable waves such as body waves, higher modes of surface wave, and noise. These waves can affect the interpretation of the shear wave profile if not accurately controlled. Additionally, there is a lower limit to imaging thin layers and small structures in surface wave methods. In the same way, the thin beds and small structures might cannot be mapped by using a resistivity survey, except when they produce an exceptionally high resistivity contrast with the surrounding stratigraphy. As a result of these limitations and because seismic surveys rely on various physical properties than resistivity surveys, combining the two methods may provide crucial cross-checks that will lead to better interpretation.

Particularly in electrical methods, electrical resistivity tomography (ERT) has become commonly used to investigate the shallow subsurface in karst terrains because of the high resistivity contrast that exists between the air-fill voids and the surrounding layers. If the void features are dried, then the resistivity is high, whereas the resistivity will decrease if the voids are filled with clay or water (Chalikakis et al., 2011). Two-dimensional ERT surveys have several electrode configurations, such as Wenner, Schlumberger, dipole-dipole and, pole-dipole. Determining which of these arrays can provide an appropriate result in karst feature relies on the depth of investigation, the sensitivity to vertical or horizontal variations, and the impact of noise (Loke, 2001; Zhou et al., 2002). Moreover, several non-invasive surface wave methods, such as spectral analysis of surface waves (SASW) (Stokoe et al., 1994), multichannel analysis of surface waves (Park et al., 1998), and microtremor analysis method (Okada, 2003), have been

widely employed to evaluate in-situ shear wave velocity profile. The most popular method currently utilized is the multichannel analysis of surface waves (MASW). The MASW method is a recent seismic method that uses the ground roll, or surface wave, to estimate the in-situ shear wave velocity of the shallow underground (Choon et al., 1999). In fact, this is a very suitable method for karst terrain areas since the differences in shear wave velocity can be employed to distinguish between unconsolidated soils and bedrock.

1.2. AIM OF STUDY

The primary objective of this research is to evaluate the electrical resistivity tomography (ERT) method integrate with the multichannel analysis of surface waves (MASW) in order to enhance characterization of the subsurface. Specific objectives are 1) to image the subsurface in the study area to a depth of 70 feet; 2) to compare the ERT images generated using both the dipole-dipole and Wenner-Schlumberger arrays; 3) to assess how variations in the MASW array configuration affected MASW data quality; and 4) to compare the ERT-estimated depth to top-of-rock and the MASW-generated depth to top-of-rock.

1.3. PREVIOUS RESEARCH

In the last few years, couple of studies have been accomplished to supply strategies for subsurface geophysical techniques in complex karst terrain. These studies illustrate the benefit of using multichannel analysis of surface wave (MASW) and electrical resistivity tomography (ERT) in combination. Additionally, they point out the strengths and the weaknesses of these methods.

According to Thitimakorn et al. (2013), 2D-resisitivity imaging and 2D-MASW were assessed for their ability to provide accurate subsurface data for sand and gravel

deposit exploration within a suitable cost and timeframe. Both the seismic shear velocity profile and 2-D resistivity image profile indicated a perfect resolution for images of the soil units and a perfect correlation with the borehole data, but the 2D-resistivity technique provided a superior lateral variation in the underground image. Moreover, the 2D-resistivity was obtained with 48 electrodes and 5 mm electrode spacing provided a greater depth of penetration to 35 m. Alternatively, the 2D-MASW data provided a slightly lower depth of penetration to 25 m. The 2D-resistivity method had the least time and highest cost per survey, while the 2D-MASW method had a high cost of tools and operational time (Thitimakorn et al., 2013). In fact, the 2D-resistivity imaging technique was superior to the MASW technique for investigating the sand deposit in the study area.

Kidanu et al. (2016) imaged the underground morphology of an active cavity in Green County, Missouri by using electrical resistivity tomography (ERT), multichannel analysis of surface waves (MASW), and borehole information, for purpose of understanding long-period effect and designing efficient reduction measures. The research illustrates that sinkholes arose over a surface-water drainage pathway and were distinguished by a visible zone of low resistivity (Kidanu et al, 2016).

Nwafor (2015) completed a study on imaging the subsurface of karst terrain area to 50 ft by utilizing multichannel analysis of surface waves (MASW) and electrical resistivity tomography (ERT) in Newburg, Missouri. The purpose of this study was to determine an optimum acquisition of MASW method and to contrast the evaluated top of bedrock from the MASW and ERT data sets. The results of the comparative interpretation of the MASW and ERT data, indicated that the depth of bedrock, which was determined by geophone interval of 2.5ft and 5ft in the MASW technique, was

consistent with ERT information. In addition, the most suitable parameters that gave an accurate result for evaluating the top of bedrock and for imaging the subsurface to 50ft were 5ft geophone spacing at 20ft offset and 5ft geophone spacing at 40ft offset. It was suggested to use 2.5ft geophone spacing if the depth target is about 40ft, and 5ft geophone spacing at 20ft shot offset distance if the depth target is about 80ft (Nwafor, 2015).

Torgashov (2012) conducted research that generated the first geophysical subsurface maps of the depth to top of rock, solution-widened joints, and groundwater in the Lane Spring Recreational Area by using electrical resistivity tomography (ERT) and multi-channel analyses of surface waves (MASW). The study area is an alleviated type of spring and flows form a branch of the Little Piney Creek. This area is located in karst terrain and has a structurally complex geology relied on the Interpretation result of the ERT, MASW and restricted well log information. This complexity made the MASW method ineffective for imaging the karst features in this study area. On the other hand, the MASW method was capable for imaging a groundwater, while the ERT was not efficient for such imaging, possibly due to the small variations in the resistivity between the rocks dissected by multiple solution-widened joints and the superimposed dry soil. Moreover, ERT and MASW techniques were both successful in imaging the variable depth of bedrock, but the solution-widened joints were imaged only by the ERT method because of the perfect resolution of the ERT result (Torgashov, 2012).

1.4. SELECTION OF METHODS

In view of the preceding research completed on the subject, the integration of electrical resistivity tomography (ERT) method and multichannel analysis of surface waves (MASW) method are able to create reliable results in determining depth to top- of-rock and subsurface cavity detection in karst terrain area. In addition, the qualities of usability, cost-effectiveness, well log information, and site condition, make these methods suitable for fulfilling the following objectives of this research: (1) organizing a successful acquisition for collecting both ERT and MASW data; (2) defining the perfect integration of ERT and MASW methods in order to determine depth to bedrock and to characterize the shallow subsurface image.

To complete the project objectives, electric resistivity tomography (ERT) data were acquired along three traverses with the use of two different arrays on traverse 1 namely dipole-dipole array and Wenner-Schlumberger array, while using only dipole-dipole array on traverses 2 and 3. Traverses 1 and 2 were oriented NE – SW, whereas the traverse 3 was directed N-S to cross traverses 1 and 2. On the other hand, a traverse of MASW were acquired along the middle of ERT Traverse 1 with two different array configurations. All data were acquired on the 15th of June with approximately 96 °F average temperature in the study area.

2. GEOLOGICAL SETTING

2.1. OVERVIEW

This chapter presents and discusses the geology and surficial deposit material of the study area, illustrated with relevant diagrams. A geologic overview of the stratigraphic units and structural geology of Phelps County, Missouri is discussed. A brief information about the depth to bedrocks in the study location is presented through the use of data from wells located in and nearby the study area.

2.2. SITE LOCATION

A single site was selected for this research because it has no complex topography and is close to Missouri University of Science and Technology. It is located in Phelps County in the south-central part of Missouri. Figure 2.1 illustrates the location of the study area.

The study area is located south of Interstate 44 and northwest of highway 63, about 15 miles south of Rolla, Missouri (Figure 2.2), approximately between longitude (37°48'29.21"N) and latitude (91°51'52.56"W). It has an average elevation range of 820 to 848 feet.

2.2.1. Surficial Material of the Study Area. The majority of the study site has a flat tomography with some sloped areas that are covered with grasses and trees. The area is composed of residual and alluvial deposits (Figure 2.3). These deposits are generally derived from a small layer of loess that exists on the steady terrain with soils obtained from highly cracked sandstone and dolomite bedrock on the steep side-slope of the valley (USDA, 2001). Additionally, the soils created in the residuum are from dolomite or

cherty limestone range from deep to shallow, and are composed of a high proportion of chert. Surficial and alluvium geological map of the study area indicates that there is a floodplain beside the site location (Figure 2.4).

Figure 2.1. Location of the research site in Phelps County, Missouri.

2.3. GEOLOGY AND STRATIGRAPHY

The study site is situated on the Salem Plateau Physiogeographic region of Missouri (figure 2.5), which surrounds the St. Francois Mountains and is bordered to the

southwest by the Springfield Plateau. The Salem Plateau is capped by Ordovician-age strata that is mostly composed of dolostone or dolomite. Bedrock of the study area is generally capped by sedimentary cherty dolomite, sandstone and clay strata from an early Ordovician-age that is classified as Gasconade Formation.

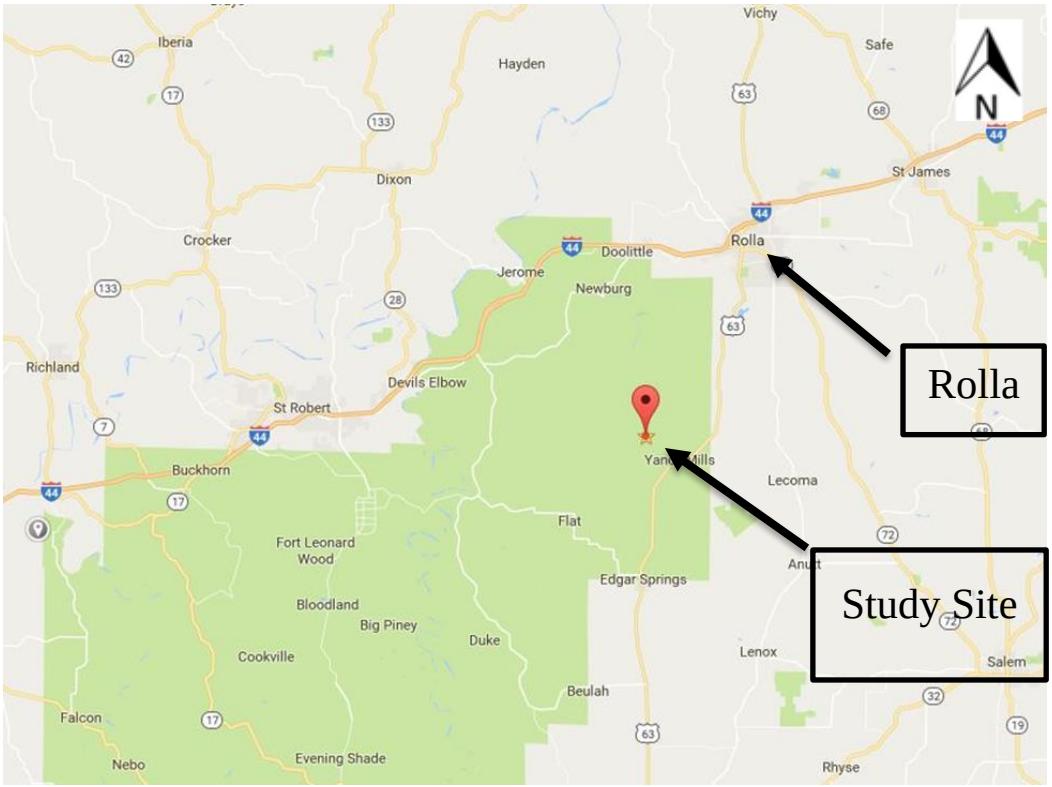

Figure. 2.2. Location of the study site approximately 15 miles south of Rolla.

2.3.1. Geologic Overview of Stratigraphic Units in Phelps County, Missouri.

Generally the subsurface stratigraphy of Phelps County is composed of enormous beds of dolomite, cherty dolomite, and sandstone along with minor deposits of limestone, shale, and siltstone. These bedrock formations are Ordovician-system deposits and consist of the following geologic units: Gasconade Dolomite, Roubidoux Formation, Jefferson City-Cotter Dolomite, and Pennsylvanian-system deposit (USDA, 2001).

Figure 2.3. The environment of the site.

Figure 2.4. Alluvium and surficial geology map of the study area (courtesy of Google Earth). The study area marked as a red square.

2.3.1.1. Gasconade Dolomite. The Gasconade Formation has a thickness that ranges between 260 to 330 feet and is comprised of enormous beds of brown to light gray dolomite with white to gray chert.

2.3.1.2. Roubidoux Formation. The Roubidoux formation is approximately 95 to 150 feet thick and consists of brown to brownish-red sandy dolomite, cherty dolomite, and sandstone (USDA, 2001). In Phelps County, an outcrop of this formation appears as sandstone and sandy dolomite bluffs and edges on hillslopes by side small stream valleys and road cuts. The surface is commonly covered by a lot of coarse sandstone fragments and chert.

2.3.1.3. Jefferson City-Cotter Dolomite. The Jefferson City-Cotter Dolomite formation is 125 to 200 feet thick and is composed of gray to brown dolomite with massive interbedded chert, sandstone, and shale layers. Because this formation is covered by soil on gently rolling ground, rock outcrops are dispersed in some places. However, places that have an enormous brown crystalline dolomite layer, crop out on hillslopes and are composed of small bluffs. Additionally, there are small glades where soil cover is thin or missing.

2.3.1.4. Pennsylvanian system deposit. The youngest bedrock, Pennsylvanian clay and sandstone, exists in the north part of Phelps County. The clay sediments are generally white to purple and are limited along with the sandstone to the wide highland divides.

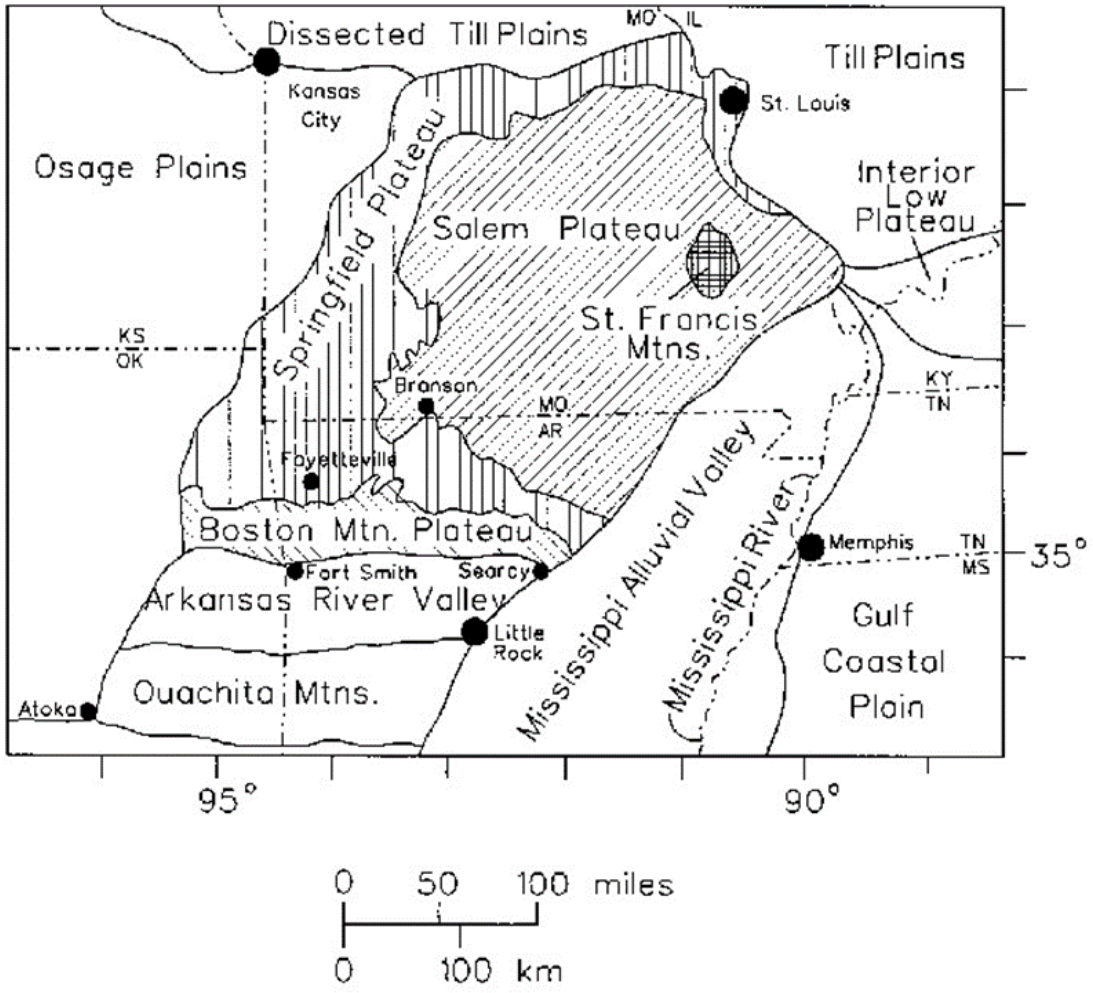

Figure 2.5. Geological map of the Ozark Plateau (Torgashov, 2012).

2.4. FAULTING

The Phelps County area has geologically old faults, with no record of recent activations even though the area is located near the infamous New Madrid seismically active zone (Figure 2.6). Additionally, sinkholes exist in the Phelps County area and more abundant in the south and the southeastern part of the county, in which the Roubidoux formation is deeply weathered.

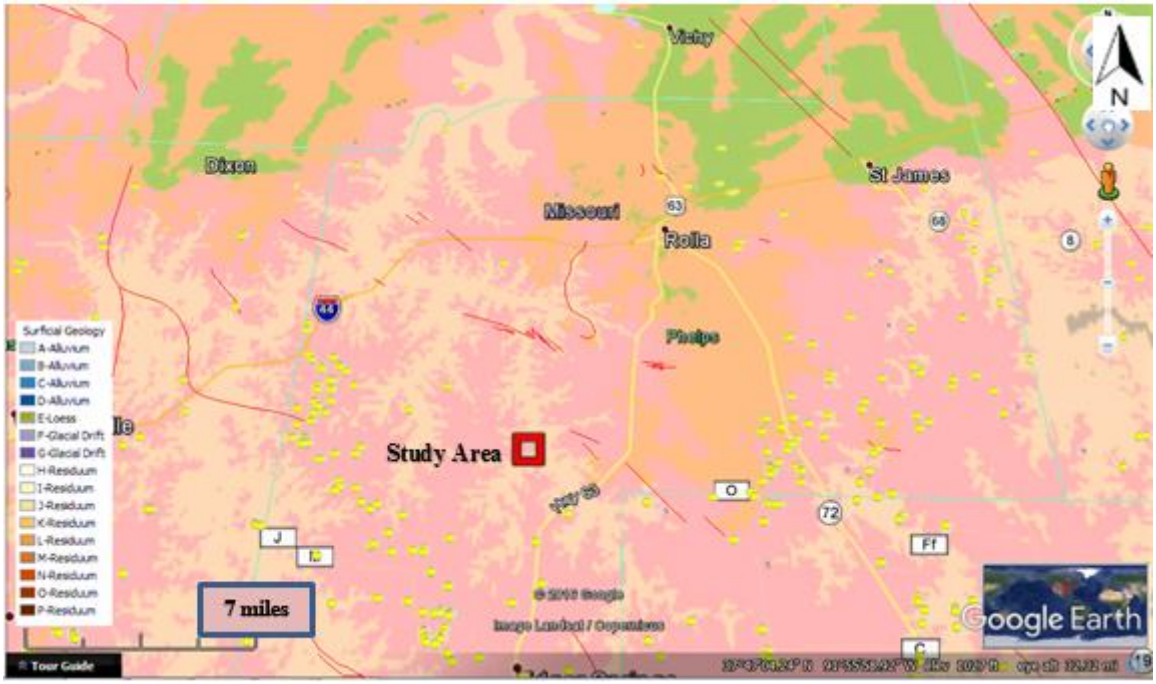

Figure 2.6. Geological map of study area (Courtesy of Google Earth). The study area is marked as red square. Mapped faults and lineaments (marked as blue lines) nearby the study area is trending mostly southeast-northwest. Yellow dots show locations of known sinkholes.

2.5. BOREHOLE DATA

A well log is available for the study area, which is located approximately 60ft from the ERT Traverse 1 and the MASW Traverse1. This well log was recorded in 2008 and the purpose of drilling this well was to obtain water for a domestic farm. The location of the well is approximately between latitude (37 °48' 29.9") and longitude (91 °51'53.0"), and it has an elevation of 830 feet. The total depth of the borehole is 212 feet and the depth to bedrock is 30 feet. The study area has other available wells, and these are located about a mile or less than mile away from the MASW and ERT survey as illustrated in figure 2.7. According to the bedrock maps of the study area obtained from the Missouri Department of Natural Resources and from the data of these wells, the depth to the bedrock in the study area ranges from 20 to 50 ft an average. And the bedrock itself

is composed of either the Gasconade Dolomite or the Roubidoux Formation at higher elevations.

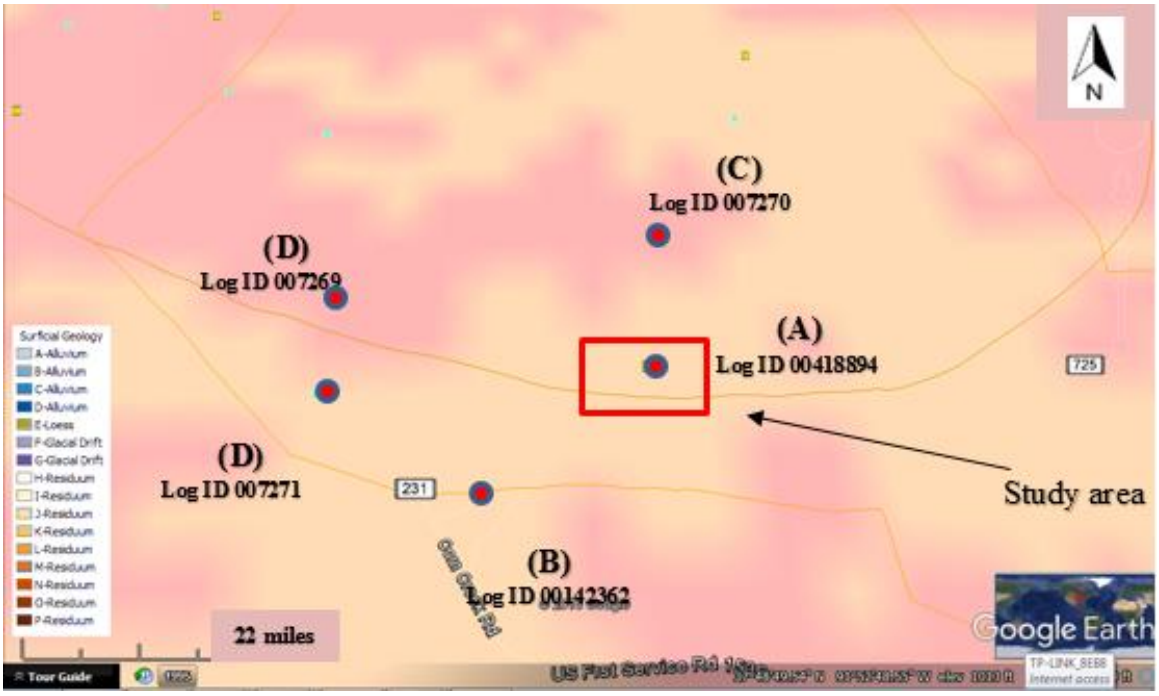

Figure 2.7. Locations of the well logs in the study area (Courtesy of Google Earth). Well log #00418894 (A) is approximately located at the study site. The other available well logs are located about less than mile away from the study area.

3. OVERVIEW OF MULTICHANNEL ANALYSIS OF SURFACE WAVES

3.1. INTRODUCTION

The multichannel analysis of surface waves (MASW) method is a non-destructive seismic technique, initially introduced by Park et al. (1999), and is widely utilized in geotechnical engineering for determining shear wave velocity and dynamic properties of subsurface materials, by evaluating the surface wave energy on the shallow subsurface. The acquisition of the MASW method came from the conventional seismic investigation technique that uses sets of receivers laid on the ground in a line. The recording data of this technique always comprises unfavorable waves like body waves, higher modes of surface waves, and ambient noise. MASW is capable of differentiating the variety of seismic waves based on wave propagation features like attenuation and velocity. In particular, the MASW uses this capability to distinguish the fundamental-mode Rayleigh wave versus the remaining of body and surface waves produced from either impulsive seismic source or natural activities such as local vehicle traffic (Park et al., 2005). The following explanation provides a discussion of basic wave theory, elastic moduli, body waves and surface waves, dispersion and phase velocity, seismic wave velocity, detailed information about MASW method, and field geometry.

3.2. SEISMIC THEORY

The main concept of seismic exploration is that an elastic wave is created at a time that is recorded precisely, and for the producing seismic waves such as P-wave, S-wave, and Rayleigh wave to travel through the subsurface media. These waves are then

refracted and reflected back to the surface where the produced waves are detected in order to obtain data about the unidentified properties of the subsurface medium (Reynolds, 2005). Obtaining knowledge of wave propagation requires a physical understanding of elastic materials and wave velocity.

3.2.1. Elastic Moduli. Earth materials are required to behave elastically so that the elastic waves transmit through the subsurface medium. The level of elasticity of materials plays a crucial role in determining the quality of wave transmission (Bormann, Engdahl, & Kind, 1999). In other words, the approach and velocity of seismic waves that travel through Earth materials are dominated by the elastic properties of the materials.

Elasticity is the behavior of a material has been subjected to a stress (force/area), change, or shape deformity (strain). However, when the stress is displaced, the materials return to its original shape. Moreover, Hooke's Law indicates that the value of strain is linearly proportional to the value of the stress, as shown in figure 3.1 (Bormann et al., 1999).

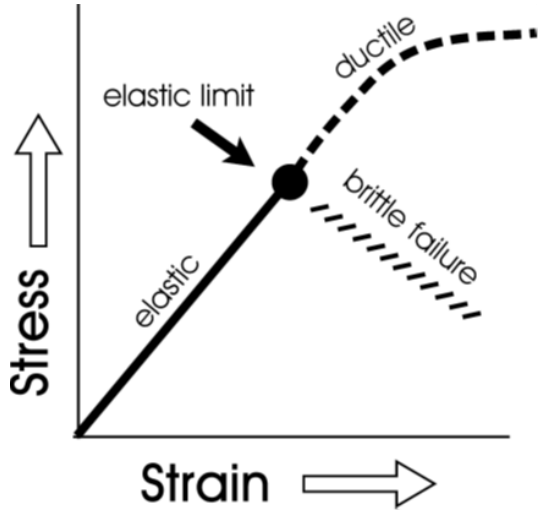

Figure 3.1. Diagram illustrating the relationship between stress and strain (Nwafor, 2015).

If an elastic material is subjected to uniaxial compression or tension, then the linear relationship between applied stress (σ) and resulting strain (ε) is given by:

$$\sigma = E\,\varepsilon, \tag{3.1}$$

Where E is the constant of proportionality, called Young's modulus, and "the strain ε isthe change in length of a line in its deformed state ($\ell\mathcal{F}$) divided by its original length ($\ell 0$).

$$\varepsilon = \frac{\ell\mathcal{F} - \ell 0}{\ell 0} = \frac{\Delta\ell}{\ell 0} \tag{3.2}$$

when a solid mass undergoes a uniaxial compression, this compression will shorten the mass in the direction of the applied stress. However, meanwhile the length of this mass will be increased in the vertical directions to the compression. Extensions in both directions can be determined, and their ratio is termed Poisson's ratio (ν):

$$\nu = \frac{\varepsilon\, 1}{\varepsilon\, 3} \tag{3.3}$$

where ν ranges from 0.05 (very hard rocks) to 0.45 (loose sediments).

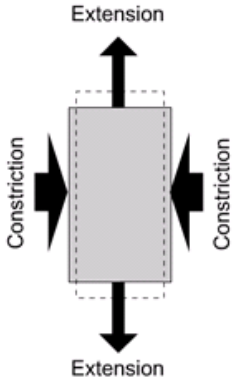

Figure 3.2. Showing the ratio of the two strains (Poisson's ratio, (ν)) (Nwafor, 2015).

The change in the volume of the symmetric material that is subjected to a comprehensive compression is further elastic coefficients. The ratio of the pressure change to the resulting comparative decline of the volume is referred to as “bulk modulus” (K). Figure 3.3 illustrates the concept of the bulk modulus.

$$K\ P = -\Delta/\Delta \tag{3.4}$$

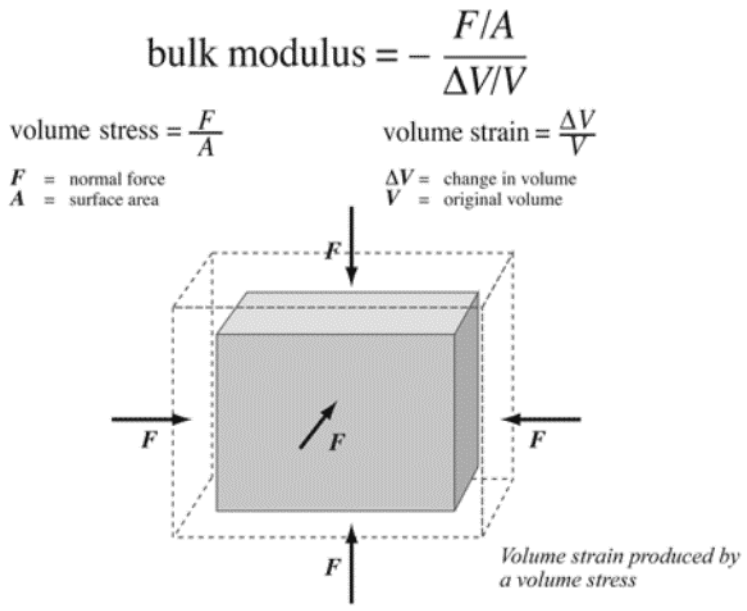

Figure 3.3. Bulk modulus is a measure of the incompressibility of the material (Nwafor, 2015).

Finally, rigidity, or shear modulus (G), is one of the parameters that can determine the seismic wave velocity. When a solid material is deformed by, small shear, a shear strain (γ) will be produced by a force of shear stress (σs), as seen in figure 3.4. The ratio of shear stress (σs) to shear strain (γ) is the rigidity modulus:

$$G = \sigma s / \gamma \tag{3.5}$$

Additionally, shear modulus (G) and bulk modulus (K) can be determined in terms of both Young's modulus and Poisson's ratio.

$$K = E / 3(1 - 2\nu) \quad (3.6)$$

$$G = E / 2(1 + \nu) \quad (3.7)$$

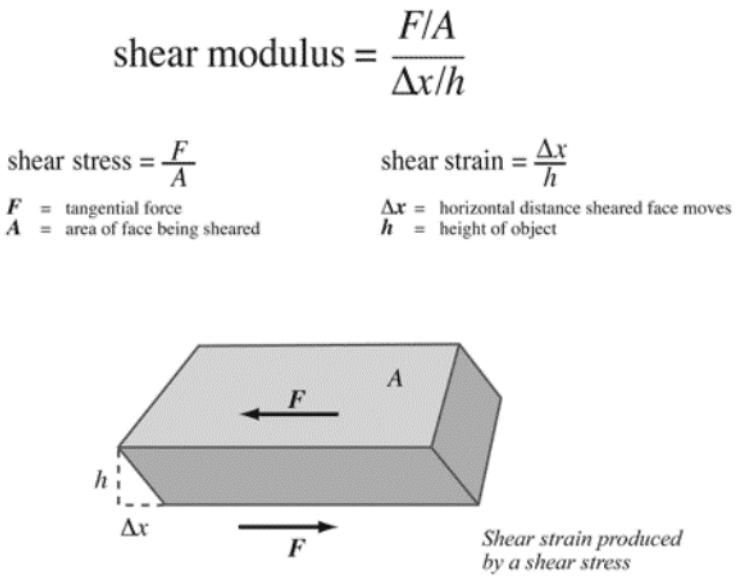

Figure 3.4. Illustrating the calculation of shear modulus (Nwafor, 2015).

3.2.2. Seismic Waves. There are various types of seismic waves, each of which has a different motion. The two essential kinds of waves are body waves and surface waves, are usually generated by activities inside the Earth's core, the movement or breakage of two masses of rocks, explosions and activities at or nearby the surface. Body waves (P-waves and S-waves) transmit through the interior of the Earth, while surface waves (Rayleigh, Love, etc.) transmit parallel to the surface and do not penetrate through the earth's interior.

3.2.2.1. Body waves. The first type of body wave is the compressional wave, or P-wave. The P-wave is the fastest type of seismic wave, and these waves are thus the first to arrive at seismic recording stations. P-waves can travel within solid and the liquid materials include water and the liquid strata of the earth. This wave has the same style of movement as a sound wave, where it moves through the rocks by pushing and pulling the rock layers.

The second type of body wave is the shear wave, or S-wave. The S-wave is slower than a P-wave and cannot travel through any liquid materials; it only passes through solid media. This feature of S-wave has led seismologists to discover that the outer core of the Earth is a liquid layer. S-waves move through solid media by shifting rock particles up and down.

The particle motion associated with P-wave is parallel to the direction in which the wave is penetrating and this motion causes a variation in aspect ratio and extension of elementary volume particles (Figure 3.5). Conversely, the particle motion of S-wave is perpendicular to the direction in which the wave is traveling. This perpendicular motion causes a change in shape and shear distortion of volume components within the medium (Everett, 2013).

3.2.2.2. Surface waves. Surface waves are seismic waves that propagate at the interface of two media. They have a lower frequency than body waves, and they arrive after body waves at seismic recording stations. The amplitude of surface waves decline significantly with depth, and most of seismic waves are limited nearby the ground. Therefore, the propagation is affected typically by shallow materials. Surface waves are divided into two essential kinds: Rayleigh waves and Love waves.

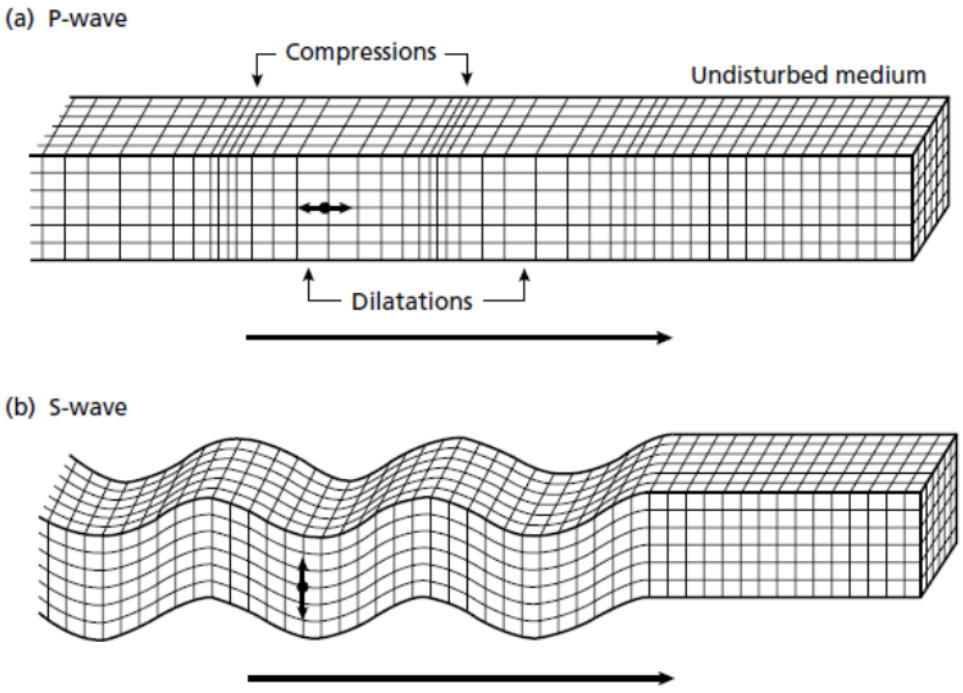

Figure 3.5. P-waves and S-waves traveling through a medium (Kearey, Brooks &Hill, 2002).

The Rayleigh waves or (ground roll), are surface waves that roll along the earth's surface like ripples seeing in the water. This motion moves the earth's surface from side to side and up and down in the same direction in which the wave is traveling. Rayleigh waves are discussed further in the sections that follow. The love waves are the fastest surface waves that move the earth's surface from side to side. Love waves are also restricted to the surface of the crust and have the larger amplitude than Rayleigh waves.

Rayleigh waves are produced by the interface between P-waves and S-waves, and the associated particle motion of Rayleigh waves is retrograde elliptical near the ground. This motion changes to prograde elliptical as the depth increases, and this motion is restricted only to a vertical plane constant with the propagation direction. Conversely,

Love waves are composed of horizontally polarized S-waves, and the particle motion of Love waves is perpendicular to the direction of the propagation (Everett, 2013), as illustrated in Figure 3.6.

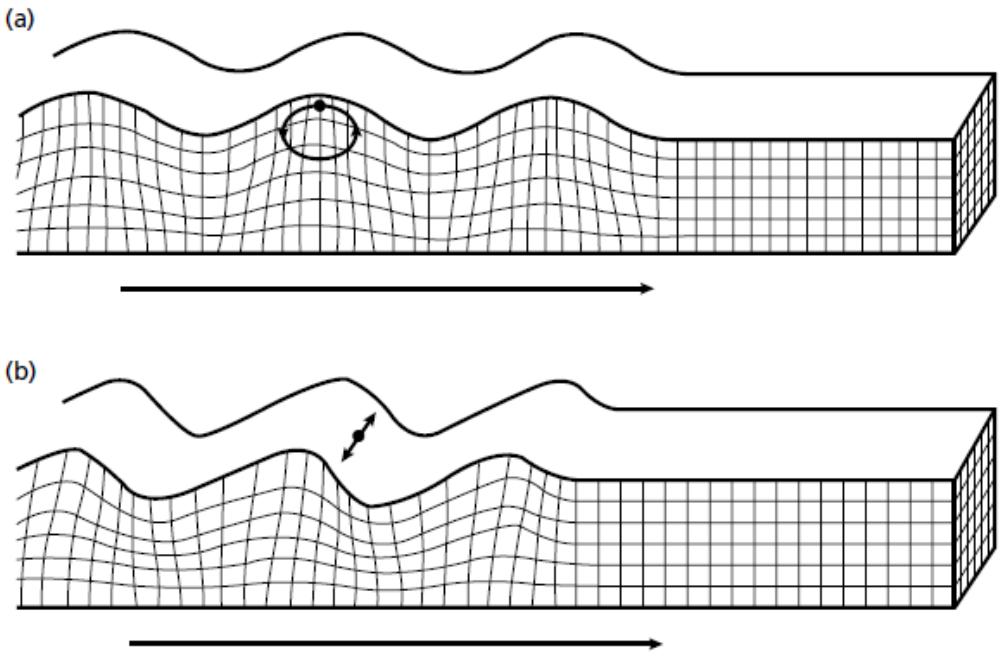

Figure 3.6. Ground particle motions associated with the motion of surface waves: (a) Rayleigh wave, (b) Love wave (Kearey et al., 2002).

Rayleigh waves (principally ground roll) are generated and recorded through the use of vertical seismic source such as sledgehammer impact or a vibrating plate and vertical receivers (geophones) (Park et al., 1997). This type of source will radiate a pack of elastic waves which includes P-waves, S-waves, and Rayleigh waves. Approximately two-thirds (67%) of the elastic waves will be generally imparted to Rayleigh waves, whereas 26% will be imparted to shear waves (S-wave), and 7% into compressional waves (P-waves) (Everett, 2013).

Rayleigh waves transmit along or near the surface of the ground with a relatively high amplitude and low frequency (Xia, Miller, & Park, 1999). The amplitude of Rayleigh waves declines rapidly with depth, and more Specifically, the amplitude will decrease to less than 30% of its initial value when penetrating to a depth that is parallel to one wavelength (Figure 3.7) (Everett, 2013).

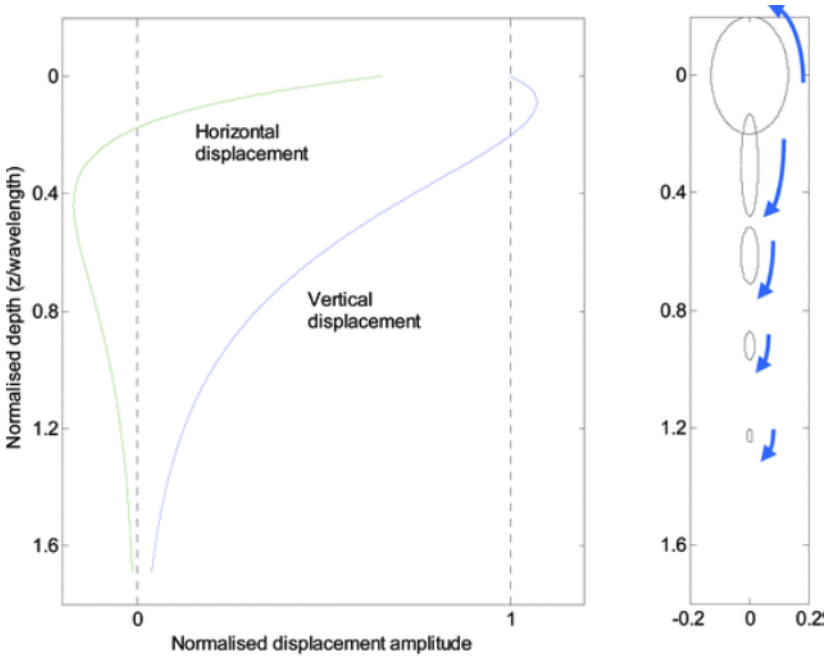

Figure 3.7. Displacement amplitude (left) and vertical particle motion (right) of Rayleigh waves as a function of depth (Gedge & Hill, 2012).

3.2.2.2.1. <u>Dispersion and phase velocity.</u> Rayleigh wave have a crucial property, called dispersion property, that can be beneficial for concluding the elastic properties of the shallow subsurface (Park et al., 1999). “This dispersion property is that wavelengths have different propagation velocities and penetration depths” (Park et al., 1995). In homogeneous half-space, Rayleigh waves are not dispersive. However, if there are two layers a heterogeneous medium, and the wavelengths of Rayleigh waves are in the range

of 1 to 30 times the thickness of the layers, then the Rayleigh waves would be dispersive (Xia et al., 1999).

Seismic sources typically generate a variation of velocity with frequency or wavelength. The propagation velocity of each harmonic frequency component is called phase velocity (Everett, 2013; Park et al., 1997). Generally, the depth penetration of surface waves relies on their wavelengths. Shorter wavelengths (with higher frequency) penetrate shallower depths with a phase velocity impacted only by the elastic properties of near surface, while longer wavelengths (with lower frequency) penetrate greater depths with a phase velocity impacted by a set of elastic properties from down to deeper layers (Figure 3.8).

3.2.3. Seismic Wave Velocity. The velocities of body wave depend on the elastic properties of the subsurface through which the waves propagate. This relationships is widely used in geophysical surveys to obtain data about the spatially distributed mechanical properties of subsoil sites (Everett, 2013). Specifically, the shear wave velocity is highly relied on when determining the shear modulus (G), which is considered to be a significant parameter in determining the soil behavior beneath any type of dynamic loading, such as vibration, and earthquakes.

Seismic velocities of body waves are defined by:

$$\mathrm{Vp} = \sqrt{\frac{K+\left(\frac{4}{3}\right)G}{\rho}} = \sqrt{\frac{E}{\rho}}\frac{(1-\nu)}{(1-2\nu)(1+\nu)} \tag{3.8}$$

$$\mathrm{VS} = \sqrt{\frac{G}{\rho}} = \sqrt{\frac{E}{\rho}}\frac{1}{2(1+\nu)} \tag{3.9}$$

where Poisson's ratio (ν) is less than or equal 0.5 and the values of the bulk modulus (K) and the shear modulus (G) are always positive. This demonstrates that P-waves velocity is always greater than the S-wave velocity. Therefore, obtaining the ratio by simplifying the two previous equations yield:

$$\frac{Vs}{Vp} = \sqrt{\frac{1/2-\nu}{1-\nu}} \tag{3.10}$$

The shear-wave velocity (S-wave) in liquids is zero because shear forces are equal to zero in liquids (G = 0).

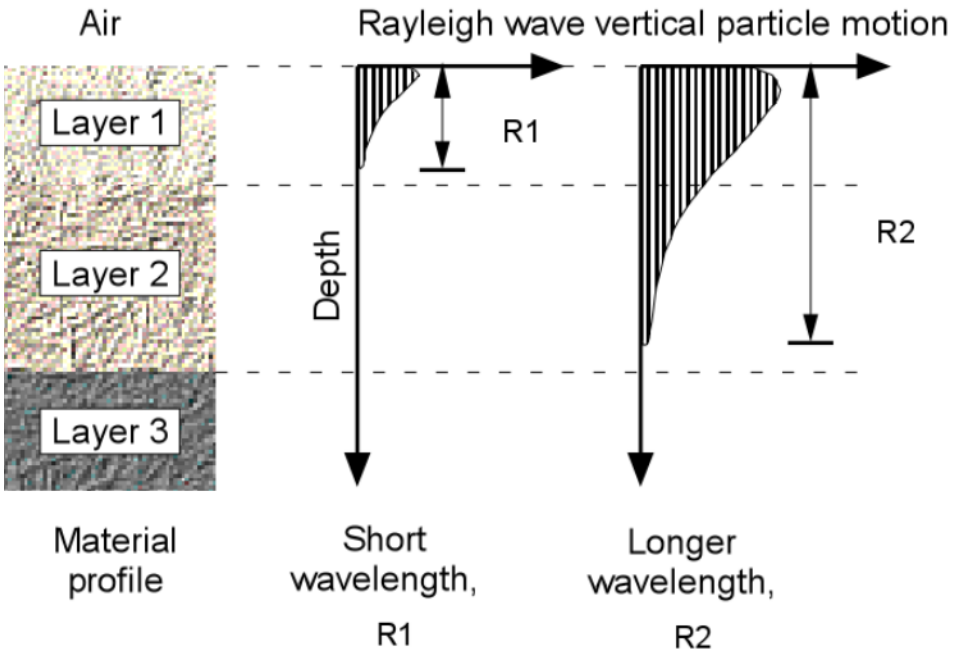

Figure 3.8. Rayleigh wave penetrations for a 3-layer model, longer periods sample deeper material and arrive before shorter periods (Martin, 2009).

Rayleigh wave velocity (VR) is less than the S-wave velocity (VS). The relation between these waves relies on the mechanical properties of the wave medium. In case of

symmetrical elastic solids, Bergman found the following equation to approximate the Rayleigh wave velocity (Ólafsdóttir, 2014) :

$$VR = \frac{0.87+1.12\nu}{1+\nu} vs \quad (3.11)$$

For a material with Poisson's ratio ν = 0.3, the approximated Rayleigh wave velocity is:

$$VR = 0.93VS.$$

Some generalized relations between seismic wave velocities are:

Vs = 0.6Vp for crystalline rocks,

0.5 s p V = V for sedimentary rocks,

0.4 s p V = V for soils and unconsolidated materials,

And 0.9 R s V = V (R V = Rayleigh wave velocity)

(Burger et al., 2006).

3.3. MASW

Multichannel analysis of surface waves (MASW) is a common method for determining shear wave velocity on the field for in order to evaluate the engineering properties of subsurface material and near-surface characterization. Surface waves comprise approximately 60% of total waves generated from the propagation of acoustic waves, and these waves can be utilized to generate shear waves velocities through a process called inversion, which transforms surface wave velocities into shear wave velocities. The shear wave (Vs) can be determined by measuring the phase velocity of Rayleigh waves, which is considered to be approximately 92% of the shear wave velocity.

3.3.1. General Procedure. The MASW method analyzes the surface waves to obtain the S-wave velocity depth profile. The procedure of this analysis can be divided to three main steps: data acquisition, data processing (determination a Rayleigh wave dispersion curve [phase velocity vs. frequency]) and Inversion analysis (determination of a layered shear wave velocities profile from the constructed dispersion curve).

3.3.1.1. Data acquisition. The acquisition of the MASW method uses a set of receivers (usually 24 or more) laid on the ground in a line with equal spacing between receivers, and connected to a seismograph in order to record the seismic data as illustrated in Figure 3.9. A sledgehammer is utilized as a source that impacts the metal plate to generate waves that can be recorded by receivers (geophones) as a function of time.

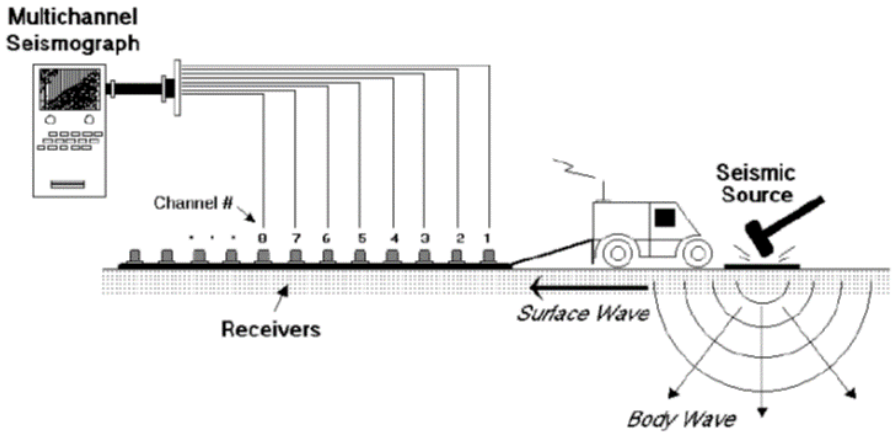

Figure 3.9. A typical MASW configuration (Park et al., 2001).

Field Geometry of MASW, Rule of thumb represents a relation of array length, source offset and maximum depth of Vs estimation, the array length equals the maximum

depth of investigation (receiver spread size D = Zmax. and the source offset is similar or smaller, as little as D/6 (Heisey, et al., 1982). However, the receiver spacing (dx) is associated to the shortest measureable wavelength and thus the shallowest resolvable investigation depth (min Z):

$$d \approx Z. \tag{3.12}$$

The source offset (x1) between the source and nearest receiver dominates the level of contamination by the near-field effects (Park et al., 2002). Table 3.1 illustrates optimum ranges of all the acquisition parameters (Penumadu & Park, 2005).

Table 3.1: Optimum Acquisition Parameters — Rules of Thumb (Penumadu & Park, 2005).

Material Type* (V_s in m/sec)	x_1 (m)	dx (m)	x_M (m)	Optimum Geophone (Hz)	Optimum Source+ (Kg)	Recording Time (ms)	Sampling Interval (ms)
Very Soft ($V_s < 100$)	1 – 5	0.25 – 0.5	≤ 20	4.5	≥ 5.0	1000	1.0
Soft ($100 < V_s < 300$)	5 – 10	0.5 – 1.0	≤ 30	4.5	≥ 5.0	1000	1.0
Hard ($200 < V_s < 500$)	10 – 20	1.0 – 2.0	≤ 50	4.5 – 10.0	≥ 5.0	500	0.5
Very Hard ($500 < V_s$)	20 – 40	2.0 – 5.0	≤ 100	4.5 – 40.0	≥ 5.0	500	0.5

* Average properties within about 30-m depth range
\+ Weight of sledge hammer

3.3.1.2. Data processing. The first step is analyzing the field records in the greatest potential range of frequencies and phase velocities. From these records, an overtone image is created that illustrates the relationship between phase velocity and

frequency for the waves that are recorded by the receiver line. These waves contain fundamental and higher modes of surface waves, and direct body waves (Park et al., 2004). Additionally, the accuracy of picking the dispersion curve is the most crucial step in order to generate an accurate result of the shear-wave velocity profile in the inversion step (Park et al., 1999).

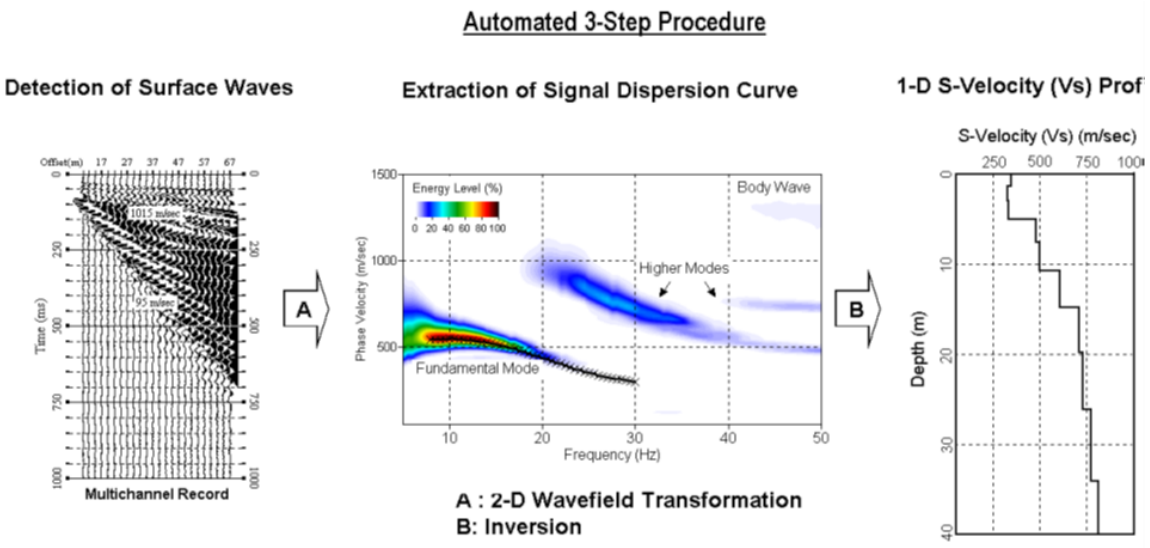

Figure 3.10. MASW data processing showed by an actual field data set acquired near Yuma, Arizona (Penumadu & Park, 2005).

3.3.1.3. Inversion analysis. The inversion step is calculated a 1-demisional shear wave velocity profile curve (at mid station) from the picked dispersion curve. This is done by utilizing an iterative inversion process that demands the dispersion data and estimations of Poisson's ratio, as well as the density (Park et al., 1999). The software program"SurSsis4" is used for processing the entire steps of MASW data (processing software developed by Kansas Geological Survey). Additionally, for generating a 2-D shear-wave velocity profile of the subsurface, combining the acquisition of multiple records with a changed source-receiver configuration as soon in Figure 3.11.

3.3.1.4. MASW data interpretation. Interpretation of MASW involves knowing the S-wave velocities variations of subsurface materials that can determine the elastic properties of the materials. For instance, bedrock or hard type of rocks have higher shear wave velocities than subsurface materials like soils. In Missouri State, the S-wave velocity value allocated to determine the depth to top of bedrock is generally 1000ft/sec. However, this value can be varied and the S-wave velocity value can exceed 2000ft/sec. Table 3.2 illustrates a general classification of subsurface materials depends on their shear wave velocity values.

Table 3.2. National Earthquake Hazard Reduction Program(NEHRP) site classification chart for different geological materials (Nwokebuihe, 2014).

Site Class	Soil Profile Name	Average Properties in Top 100 feet (as per 2000 IBC section 1615.1.5) Soil Shear Wave Velocity, V_s	
		Feet/second	Meters/second
A	Hard Rock	$V_s > 5000$	$V_s > 1524$
B	Rock	$2500 < V_s \leq 5000$	$762 < V_s \leq 1524$
C	Very dense soil and soft rock	$1200 < V_s \leq 2500$	$366 < V_s \leq 762$
D	Stiff soil profile	$600 < V_s \leq 1200$	$183 < V_s \leq 366$
E	Soft soil profile	$V_s < 600$	$V_s < 183$

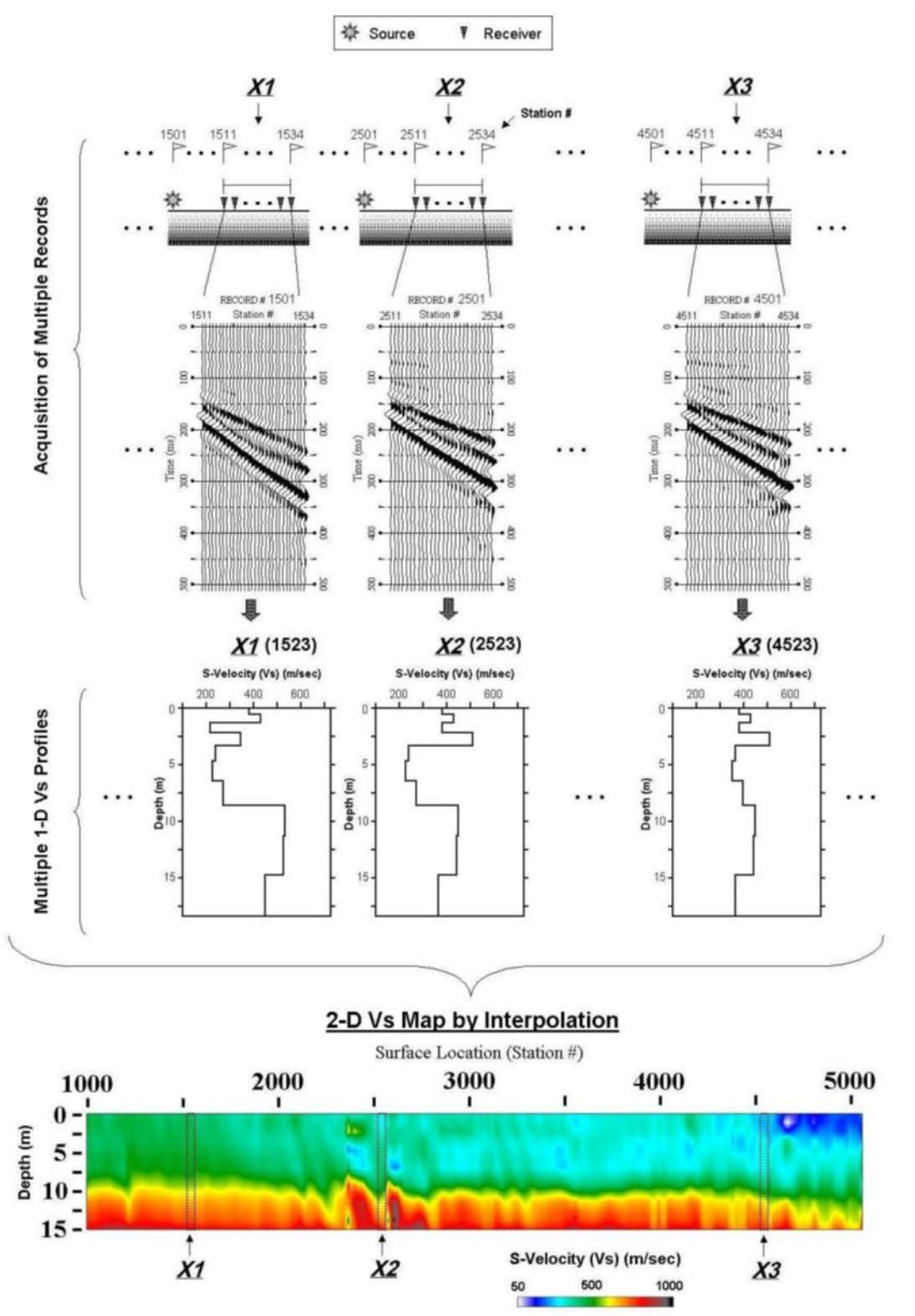

Figure 3.11. Overall procedure to generate a 2-D Vs map from the MASW (Penumadu & Park, 2005).

4. ELECTRICAL RESISTIVITY TOMOGRAPHY METHOD

4.1. INTRODUCTION

Electrical resistivity tomography (ERT) is a nondestructive geophysical method, is widely utilized for imaging the shallow subsurface in karst terrains. This technique measures the spatial variation in the resistivity of the subsurface materials such as soil and rock. The idea behind this technique is that the electrical resistivity of sock/soil materials is various because of the various geological parameters that like the mineral content, porosity, permeability and degree of water saturation in the rock.

4.2. BASIC RESISTIVITY THEORY

In 1872, George Simon Ohm derived the fundamental physical law that is used in resistivity surveys and called Ohm's law. This law is governed the flow of current in the ground. Ohm's law equation in vector form for current flow in a continuous medium is given by:

$$J = \sigma E \tag{4.1}$$

where (J) is the current density, the electric field intensity and σ is the conductivity of the medium. Practically, the electric field is measured. In case of geophysical survey the medium resistivity ($\boldsymbol{\rho}$), which is the inverse of conductance ($\boldsymbol{\rho} = 1/\sigma$), is more usually utilized. The relationship between the electric potential and the field intensity is given by

$$E = -\nabla\Phi \tag{4.2}$$

The outcome of simplifying equations (4.1) and (4.2),

$$J = -\sigma \nabla\Phi \tag{4.3}$$

Most of all surveys, the current sources possess the form of point sources. In this instance, over an elemental volume ΔV surrounding the current source I, situated at (xs, ys, zs), the 11 relationship between the current density and the current (M. H. Loke, 2001)is given by:

$$\nabla J = \left(\frac{I}{\Delta V}\right) \delta(x-x_s)\, \delta\,(y-y_s)\, \delta\,(z-z_s) \tag{4.4}$$

where (d) is the Dirac delta function. Equation (4.3) can then be rewritten as

$$-\nabla \bullet [\sigma\,(x, y, z)\, \nabla\varphi(x, y, z)] \left(\frac{I}{\Delta V}\right) \delta(x-xs)\, \delta\,(y-ys)\, \delta\,(z-zs) \tag{4.5}$$

This simple equation provides the potential distribution in the ground because of the point current source. Numerous techniques have been evolved to solve this equation. This is the "forward" modeling problem, in case of determining the potential which is exposed over a certain structure in the subsurface. Several analytical techniques have been developed for simple cases, like a cylinder in a homogenous medium or as a vertical fault between two zones each with a constant resistivity. In case of an arbitrary resistivity distribution, numerical techniques are superior to use (Loke, 2012).

In case of one-dimensional structure, in which the subsurface is constrained to several horizontal layers, the linear filter technique is often used (Koefoed, 1979). However, in case of 2-D and 3-D structures, the finite-difference and finite-element methods are used.

To begin with, the simplest case which has a homogeneous subsurface and a single point current source on the ground surface as shown in Figure 4.1. The current flows of this case radiate away from the point source, the potential differs reversely with the distance from the current source. The equipotential surfaces are a hemisphere form

and the current flows vertical to the equipotential surface, thus the potential in this case is:

$$\phi = \frac{\rho I}{2\pi r} \tag{4.6}$$

where r is the distance of a point in the medium (including the ground surface) from the electrode.

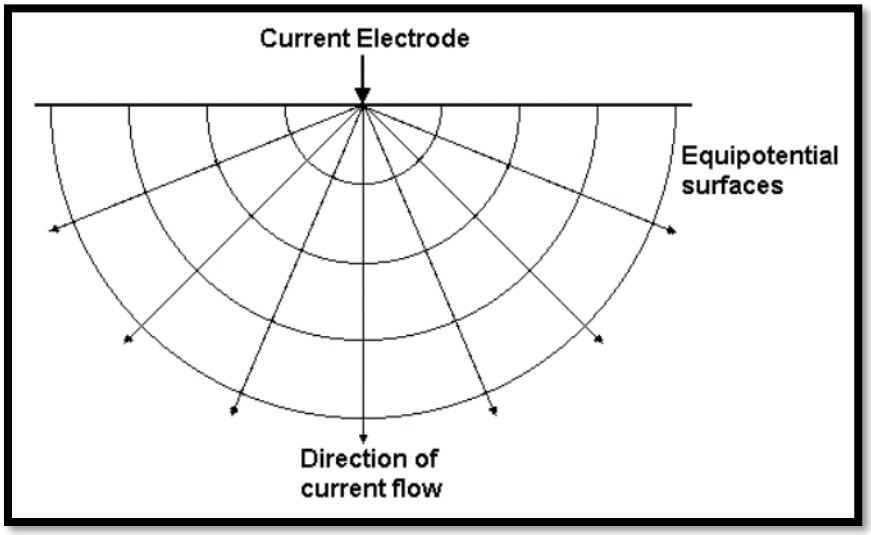

Figure 4.1. Showing the flow of current from a point current source and the potential distribution (Loke, 2012).

Practically, all types of resistivity survey minimally use two current electrodes, a positive current and a negative current source. The potential distribution caused by a pair of electrodes is illustrated in Figure 4.2. The pattern of potential values is symmetrical and almost at the mid-distance between the two electrodes. The potential value in the medium form a pair of two electrodes is:

$$\phi = \frac{\rho I}{2\pi r}\left\{\frac{1}{rc1} - \frac{1}{rc2}\right\} \tag{4.7}$$

where $(rc1)$ and $(rc2)$ are distances of the point from the first and second current electrodes.

In practice, in all of the electrical resistivity surveys, the potential difference between two points is measured. Figure 4.3 illustrates a conventional array with 4 electrodes for measuring the subsurface resistivity. Equation 4.7, is given the potential difference that is measured over a homogenous half space with a 4 electrodes array.

$$\phi = \frac{\rho I}{2\pi r}\left\{\frac{1}{rc1p1} - \frac{1}{rc2p1} - \frac{1}{rc1p2} + \frac{1}{rc2p2}\right\} \tag{4.8}$$

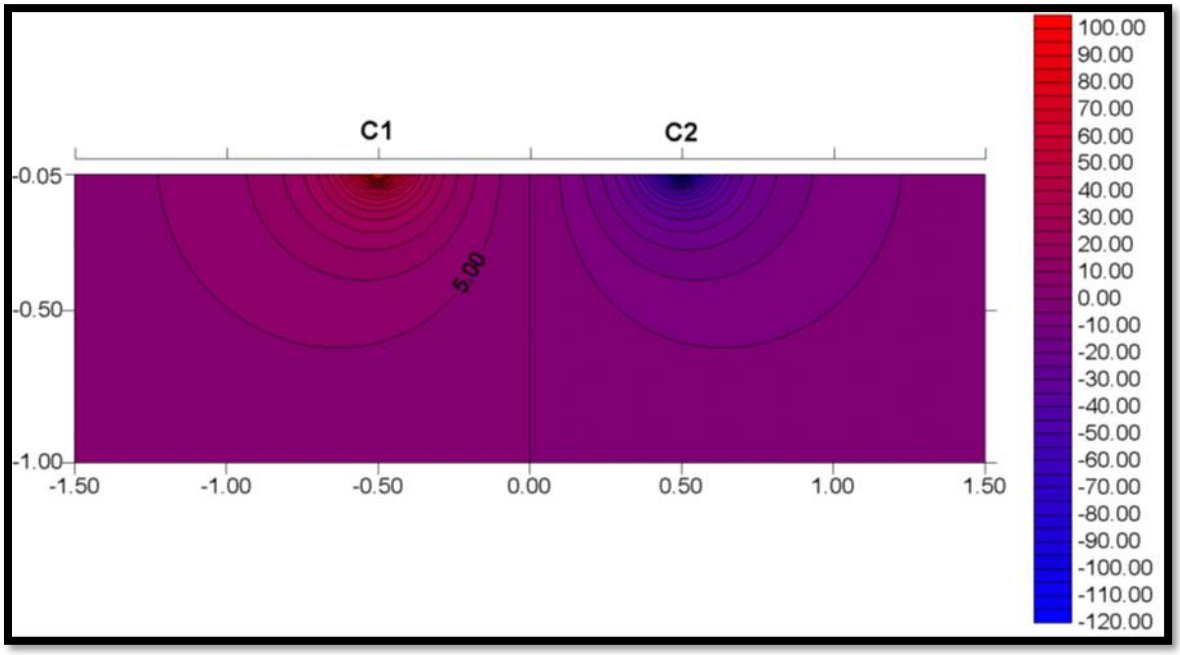

Figure 4.2. The potential distribution caused by a pair of current electrodes. The electrodes are 1 meter apart with a current of 1 ampere and a homogeneous half-space with resistivity of 1 Ohm-m (Loke, 2012).

In case of conducting a survey over an inhomogeneous medium with a 3-D distribution of the subsurface resistivity. Injecting current into the ground through the two current electrodes (C1 and C2) can measure the resistivity, and measuring the resulting voltage difference at two potential electrodes (P1 and P2) as shown in Figure 4.3. From

the potential ($\Delta\varphi$)and the current (I) values, an apparent resistivity (ρa) value can be calculated (Loke, 2012).

$$\rho a = k \frac{\Delta\varphi}{I} \tag{4.9}$$

where

$$k = \frac{2\pi}{\left\{\frac{1}{rc1p1} - \frac{1}{rc2p1} - \frac{1}{rc1p2} + \frac{1}{rc2p2}\right\}} \tag{4.10}$$

where (k) is a geometric factor, which relies on the configuration of the 4 electrodes. Resistivity measuring instrument usually provides a resistance value, $R=\frac{\Delta\phi}{I}$, thus in practice the visible resistivity value is calculated by:

$$\rho a = kR \tag{4.11}$$

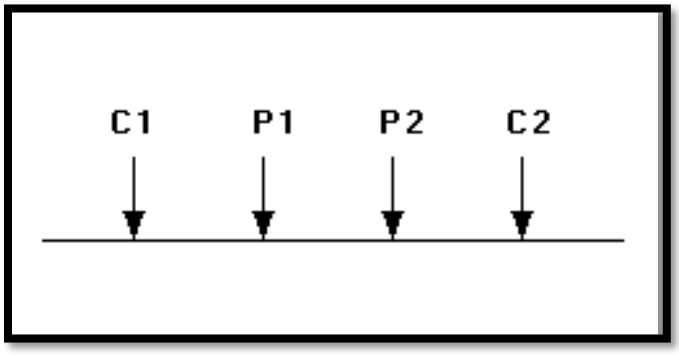

Figure 4.3. A conventional array with four electrodes to measure the subsurface resistivity (Loke, 2012).

The calculated “apparent” resistivity value is the resistivity of a homogeneous ground, which would provide the same resistance value for the same electrode configuration. However, this resistivity is not the actual resistivity of the subsurface. The relationship between the “apparent” resistivity and the “actual” resistivity is

complicated. Deriving the actual subsurface resistivity from the apparent resistivity is the “inversion” problem (Loke, 2012). The inversion technique will be discussed further in section 4.7.

4.3. PSEUDOSECTION DATA PLOTING

The pseudosection contouring technique is usually used for plotting the data from a 2-D imaging survey. In this technique, “the horizontal location of the point is placed at the mid-point of the set of electrodes used to make that measurement. The vertical location of the plotting point is placed at a distance which is proportional to the separation between the electrodes” (Loke, 1999). Another technique is to place the vertical position of the plotting point at the median depth of investigation or pseudo depth, of the electrode array used (Edwards, 1977). The pseudosection plot achieved by contouring the apparent resistivity values is an appropriate means to exhibit the data.

The pseudosection provides a very close picture to the actual subsurface resistivity distribution. Nevertheless, the pseudosection provides a deformed picture of the subsurface due to the shape of the contours rely on the sort of array used and the true subsurface resistivity(D. M. Loke, 1999). Additionally, Figure 4.4 shows how different can be the data coverage of each different arrays.

4.4. RELATIONSHIP BETWEEN GEOLOGY AND RESISTIVITY

Variation in the resistivity of the subsurface materials are mainly a function of lithology. Figure 4.5 illustrates the resistivity values of some common earth materials (Keller and Frischknecht 1966, Daniels and Alberty 1966, Telford et al. 1990).

The resistivity values of igneous and metamorphic rocks are typically high and significantly dependent on the degree of fracturing and moisture exists in the fracture. Therefore, the resistivities of igneous and metamorphic rocks vary from approximately about 1,000 to 10 million Ohm-m, relying on moisture level. However, sedimentary rocks are usually more porous and have higher moisture. Thus usually have lower resistivity than the igneous and metamorphic rocks. The resistivity values of sedimentary rocks range from 10 to about 10,000 Ohm-m, with massive values below 1,000 Ohm-m.

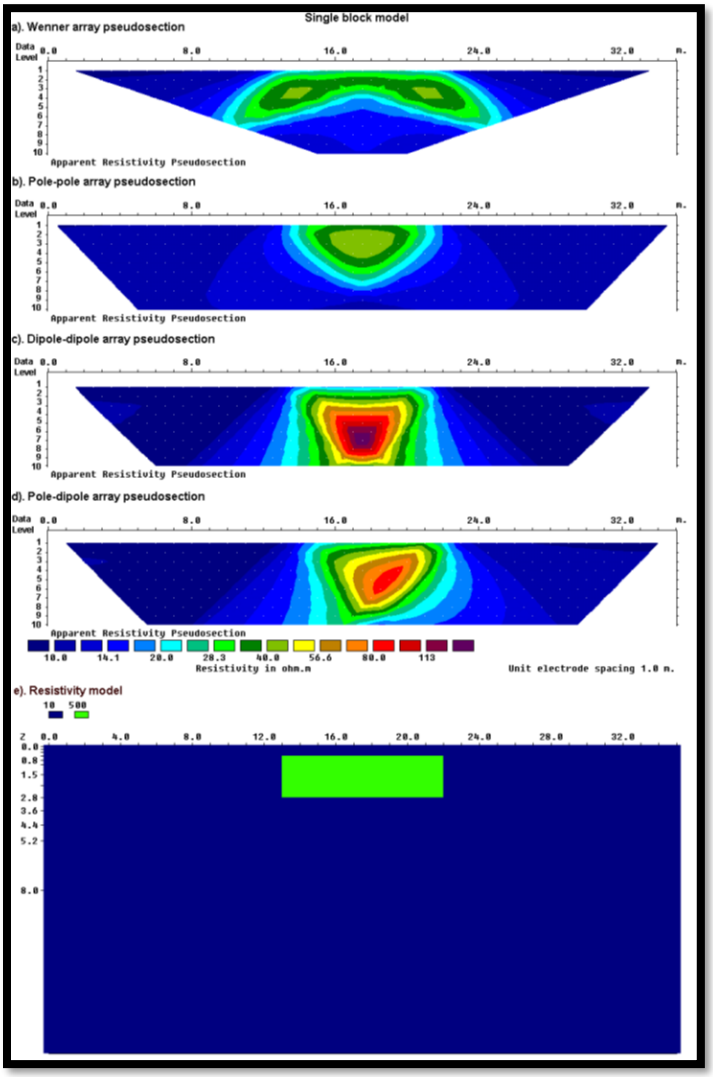

Figure 4.4. The apparent resistivity pseudosections from 2-D imaging surveys with different arrays over a rectangular prism (Loke, 2012).

Unconsolidated sediments typically have lower resistivity values than sedimentary rocks, ranging from about 10 to less than 1,000 Ohm-m. Generally, the resistivity value is depending on porosity, water content and clay content. Clayey soils usually have lower resistivities than sandy soil. Nonetheless, since a certain rock or soil relies on factors like the porosity, the degree of water saturation and the concentration of dissolved salts, this causes an overlapping in the resistivity values of various rocks and soils. Additionally, Groundwater resistivity values vary from 10 to 100 Ohm-m and rely on the concentration of dissolved salts.

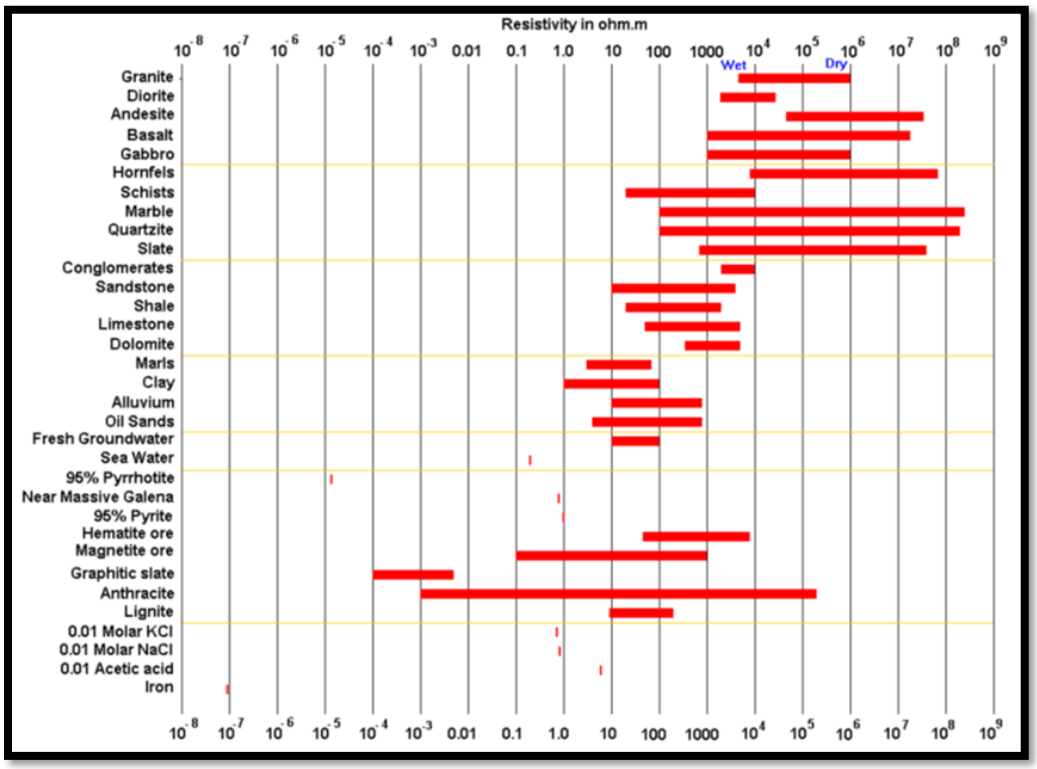

Figure 4.5. The resistivity of rocks, soils and minerals (Loke, 2012).

4.5. COMPARISON OF DIFFERENT ELECTRODE ARRAYS

Practically, the most common electrode arrays that used for 2-D imaging surveys are Wenner (Figure 4.6(a)), Schlumberger (Figure 4.6(b)), dipole-dipole (Figure 4.6(c)),

pole-dipole (Figure 4.6 (d)), and Wenner-Schlumberger (Figure 4.6(e)), Selecting the most suitable array for a field survey is depending on a type of structure to be imaged, the sensitivity of the resistivity meter and the background noise level. Moreover, some of the array features that ought to be taken into account are "(1) the depth of investigation, (2) the sensitivity of the array to vertical and horizontal changes in the subsurface resistivity, (3) the horizontal data coverage and (4) the signal strength" (M. H. Loke, 2001).

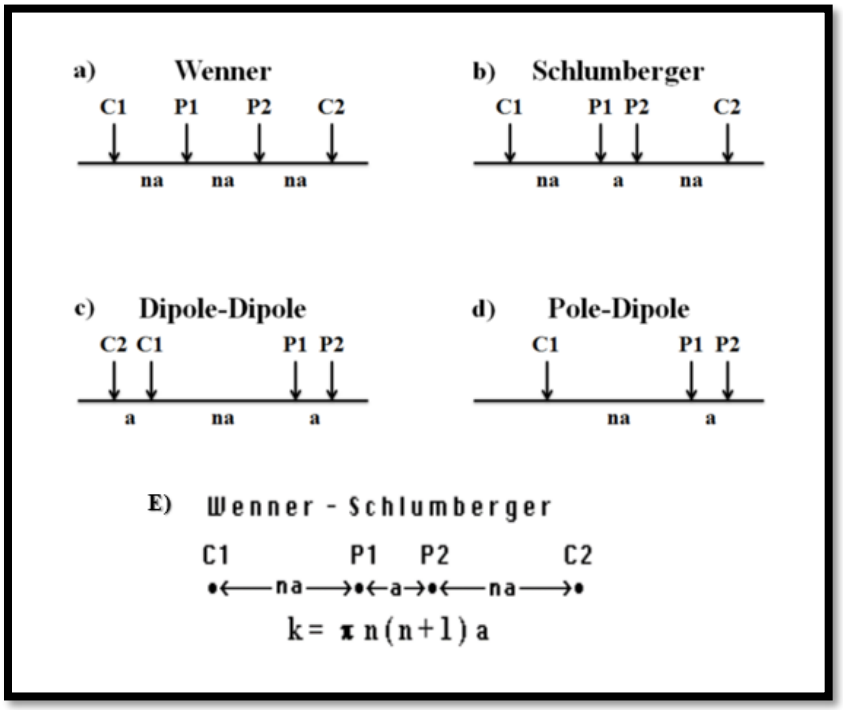

Figure 4.6. Common arrays used in resistivity surveys and their geometric factors. The Wenner (a), Schlumberger (b), dipole-dipole (c), pole-dipole (d), and Wenner-Schlumberger arrays have two parameters, the dipole length "a" and the dipole separation factor "n". While the "n" factor is commonly an integer value, non-integer values can also be used (Loke, 2011).

The Wenner array is designed for lateral profiling to calculate the resistivity of subsurface $\rho(x)$ at an approximately fixed depth of penetration (Everett, 2013). The Wanner array is proper for surveys carried in a high noisy area because of its strong

signal strength. One weakness of this array is that when the electrode spacing is increased the horizontal coverage becomes comparatively poor.

The Schlumberger array is created for vertical sounding, but its lateral resolution is limited. This array requires long wire connections that need to be moved for each measurement, which makes this array cumbersome in the field (Everett, 2013).

The dipole-dipole array has the best horizontal resolution and data coverage among other arrays. The signal strength of this array is low for large values of the “n” factor, which consider to be a possible disadvantage. However, increasing the “a” spacing between the current and the potential dipole pair of electrodes to decrease the drop in the potential, this can solve the problem (Loke, 2012). In fact, this makes the dipole-dipole array works successfully in areas like karst terrain that have major lateral variations in the subsurface.

The pole-dipole array has a lower signal strength compared with the Wenner and Wenner-Schlumberger arrays but higher than the dipole-dipole array. When a number of electrodes is restricted with measurements in both the forward and reverse directions, the pole-dipole array is a perfect choice (Loke, 2012).

The Wanner-Schlumberger array is a new combination of the Wenner and Schlumberger arrays producing from further recent work with electrical imaging surveys. In regions where both horizontal (for low "n" values) and vertical structures (for high "n" values) are predictable, this array tends to be a good compromise between the Wenner and the dipole-dipole because of its moderately sensitive to both types of geological structures. The horizontal data coverage of Wenner-Schlumberger is slightly wider than

the Wenner array data. However, it is narrower than the horizontal data coverage of with the dipole-dipole array (Loke, 2012).

4.5.1. Sensitivity Functions. The measurement of electrical resistivity tomography is sensitive to a spatial average of the shallow subsurface electrical resistivity distribution. Figures 4.7 illustrates the contour pattern for the sensitivity function of the Wenner, Wenner-Schlumberger and dipole-dipole arrays for a homogeneous earth model.

Generally, the sensitivity function indicates "the degree to which a change in the resistivity of a section of the subsurface will influence the potential measured by the array" (Loke, 1999). When the value of the sensitivity function is higher, the influence of the subsurface area becomes greater on the measurement. For all the three arrays, the greatest sensitivity values exist nearby the electrodes. The contour patterns in the sensitivity function plot are different for the various arrays at higher distances from the electrodes. This helps to describe the response of the various arrays to different types of structures(Loke, 1999).

In Figure 4.7A, the contours in the sensitivity function plot for the Wenner array is nearly horizontal below the center of the array. This property makes the Wenner array relatively sensitive to vertical changes in the subsurface resistivity beneath the center of the array. Nevertheless, in horizontal changes in the subsurface resistivity is less sensitive.

The sensitivity function plot for the Wenner-Schlumberger array (Figure 4.7b) is a little different from the Wenner array with slightly lower sensitivity values in the regions between the C1 and P1 (and as well C2 and P2) electrodes and a slight vertical curvature beneath the middle of the array. The sensitivity that is a highly concentrated beneath the

P1-P2 electrodes has high values. This indicates that the Wenner-Schlumberger array is moderately sensitive to both horizontal and vertical structures.

The sensitivity pattern for the dipole-dipole arrays in figure 4.7c illustrates that the largest sensitivity values are concentrated between the C2-C1 dipole pair and between the P1-P2 pair. This indicates that this array is the greatest sensitive to resistivity changes between the electrodes in each dipole pair. Therefore, the dipole-dipole array is very sensitive to horizontal changes in resistivity, while comparatively insensitive to vertical changes in resistivity. That indicates that it is a perfect array in imaging the vertical structure like dykes and cavities and has a poor quality in imaging horizontal structure like sills or sedimentary layers (Loke, 1999).

4.6. 2-D ERT DATA ACQUISITION

Data acquisition unit is used a SuperSting system, which is an automated unit that measures the apparent resistivity of the subsurface Figure 4.8a. For 2-D acquisition, using the SuperSting unit that involves passing electric currents through electrodes that are attached to a metal stake that is plunged to the ground, with consistent spacing between electrodes for the entire survey. The SuperSting unit can be linked to more than 60000 interconnected electrodes, only 4 electrodes are active at any one time. Each pair of electrodes works as current electrodes, whereas another set of two electrodes works as the voltage electrodes. The SuperSting unit would transmit a certain current by the two active current electrodes into the subsurface and record the corresponding potential difference (voltage) by the two active voltage electrodes. The configuration of the electrodes rely on

the standard arrays that were discussed in section 4.5. The setup scheme for a dipole-dipole array configuration is illustrated in Figure 4.8b.

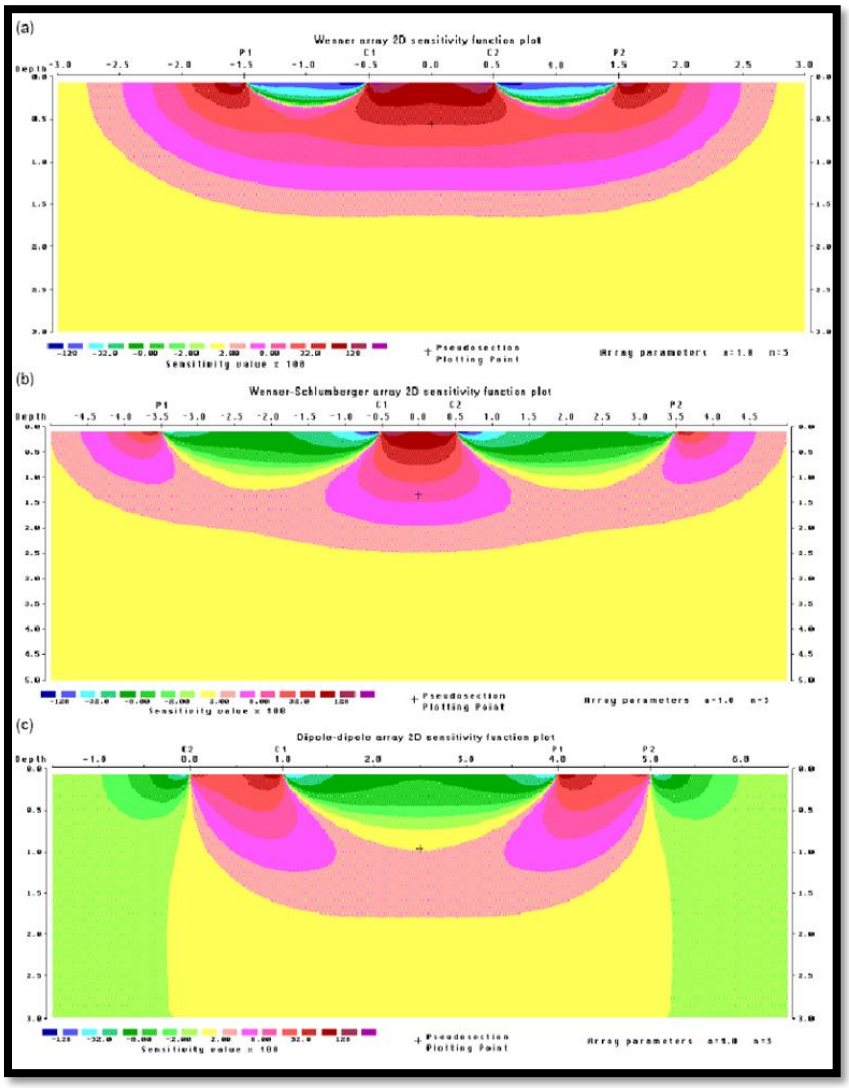

Figure 4.7. The sensitivity function or patterns for the (a) Wenner (b) Wenner-Schlumberger and (c) dipole-dipole arrays (Loke, 1999).

4.7. ERT DATA PROCESSING

After the ERT data field collected in the field, Res2DInv is used to convert the apparent resistivity values recorded from the field to true resistivity model that can be used for geological interpretation. The process of this converting is called inversion and the steps involved in this process include:

- To obtain a perfect model, the data must be of good quality. Therefore, inspecting the resistivity data for determining the bad point (data points with high or low apparent resistivity values) is a pre-inversion step that must be applied before running the inversion, as shown in a pseudosection plot (Figure 4.9a) and a profile plot (Figure 4.9b). In profile form, the bad points are standing out from the rest and can be removed manually from the data set (Loke, 2012).
- Calculating the subsurface parameters by some alterations of a computer and then generating a 2D resistivity model of the subsurface indicating the true resistivity. This 2D resistivity model shows the distribution of resistivity below the corresponding traverse. A 2D ERT cross-section is illustrated in Figure 4.10.

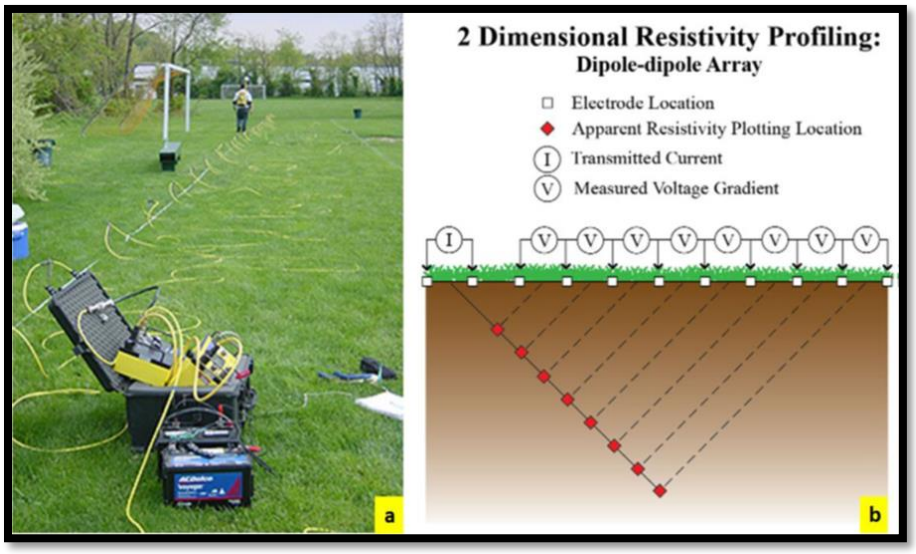

Figure 4.8. The setup of an ERT system. (a) The ERT SuperSting unit for data acquisition, the dipole-dipole array configuration. Images from the U.S. Environmental Protection Agency (2003).

During the inversion processing, the root mean square (RMS) error has to be as low as possible to increase the quality of the calculated model. An RMS error of 5% is recommended for a good quality of the geologic model (Loke, 1999).

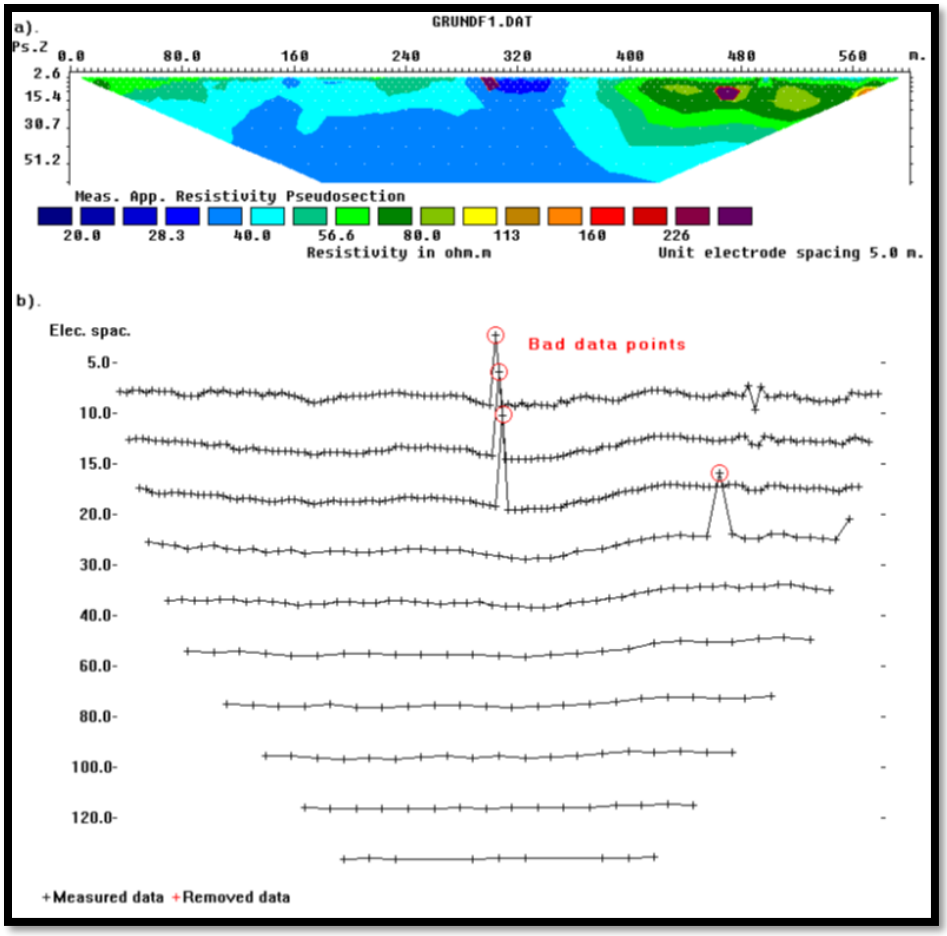

Figure 4.9. An example of a field data set with a few bad data points. The most obvious bad data points are located below the 300 meters and 470 meters marks. The apparent resistivity data in (a) pseudosection form and in (b) profile form. (Loke, 2012).

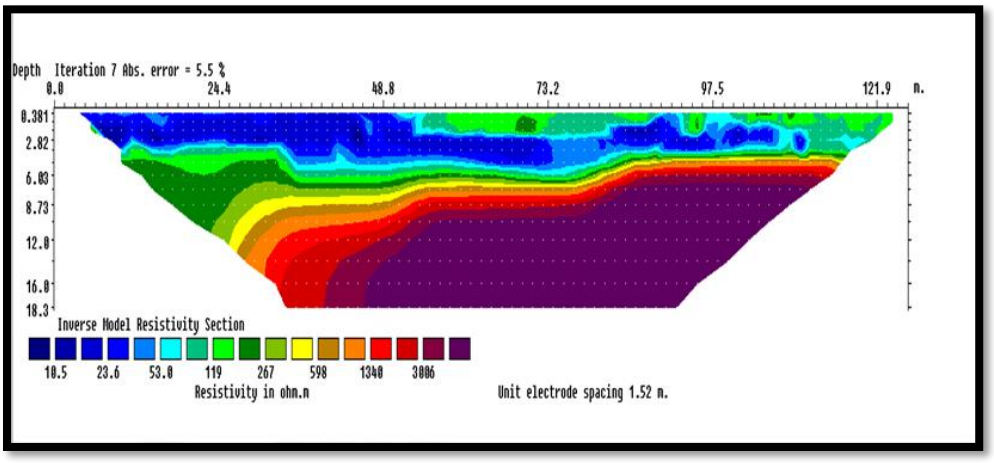

Figure 4.10. An ERT cross-section.

4.8. STRENGTHS AND WEAKNESSES OF THE ERT METHOD

The ERT is a non-destructive method and data acquisition is relatively faster: it would take an approximately 2 hours to acquire data along 400 feet traverse by 3 man crew and an extra hour to process the data. The data interpretation would be straightforward and relatively accurate if constrained. Moreover, it is a perfect technique for cavities investigation because of high lateral and vertical resolution that are essential for analyzing a karst environment. It is relatively inexpensive compared to other methods that are used for sinkhole investigation like boring.

However, acquiring the ERT data can be difficult on paved areas and in the places where is relatively difficult for the metal steaks to be attached. It works perfectly when the ground is considerable wet which enables current to flow through the ground. An air-fill void can be interpreted as a dense rock if the air filled void is surrounded by wet sand or clay, this makes the ERT Interpretations non-unique. Cultural features such as metal fences, buried pipelines, electric power lines, etc. can create problems.

5. FIELD METHODOLOGY

This chapter describes the field parameters and the equipment of MASW and ERT geophysical methods that are used in this thesis. The data processing of those methods are also discussed.

5.1. OVERVIEW

Geophysical studies were conducted at the study area using the Electrical Resistivity Tomography (ERT), and the Multichannel Analysis of Surface Waves (MASW) tools, on 15th of June, 2016 with approximately 96 °F average temperature in the study area. Photographs from the study area are illustrated in Figures 5.1 and 5.2. The details of the data acquisition and the result of data processing are discussed below.

Figure 5.1. Showing the acquisition of MASW data.

Figure 5.2. Showing the acquisition of ERT data.

5.2. MULTICHANNEL ANALYSIS OF SURFACE WAVE (MASW)

5.2.1. Acquisition of MASW Data. Multichannel analysis of surface waves (MASW) were acquired along approximately the middle of ERT travers1 with two different array configurations (Figure 5.3). The main purpose of the measurements was to determine the shear wave velocities of subsurface materials, and depth to bedrock at two different positions of ERT Traverse1. The second purpose was to evaluate how variations in the MASW array configuration affected MASW data quality.

Twenty-four geophones of 4.5Hz frequency were lined up in a straight line along the ERT traverse1 for both configurations. A 20lb. sledge hammer was utilized as an acoustic source. Three stacks of MASW data were measured for each location. For the

first configuration, the geophone interval of 5ft and three various offset distances 10ft, 20ft and 30ft were used. The array length is 115ft. For the second array configuration, the 24 geophones were placed with geophone interval of 2.5ft and three various offset distances 10ft, 20ft and 30ft. The array length is 57.5ft. Additionally, data was collected from both ends of the receiver traverse.

5.2.1.1. Equipment used for MASW. To conduct MASW method requires five elements: a seismic source, receivers, a triggering device, transmitting cables and a multichannel seismograph.

A seismic source is utilized to transfer energy to the subsurface to induce seismic activity. Practically, a source can be an impact force applied to the ground by a hammer or falling weight, a small-scale explosion, or a mechanical vibratory device. A 20lb.

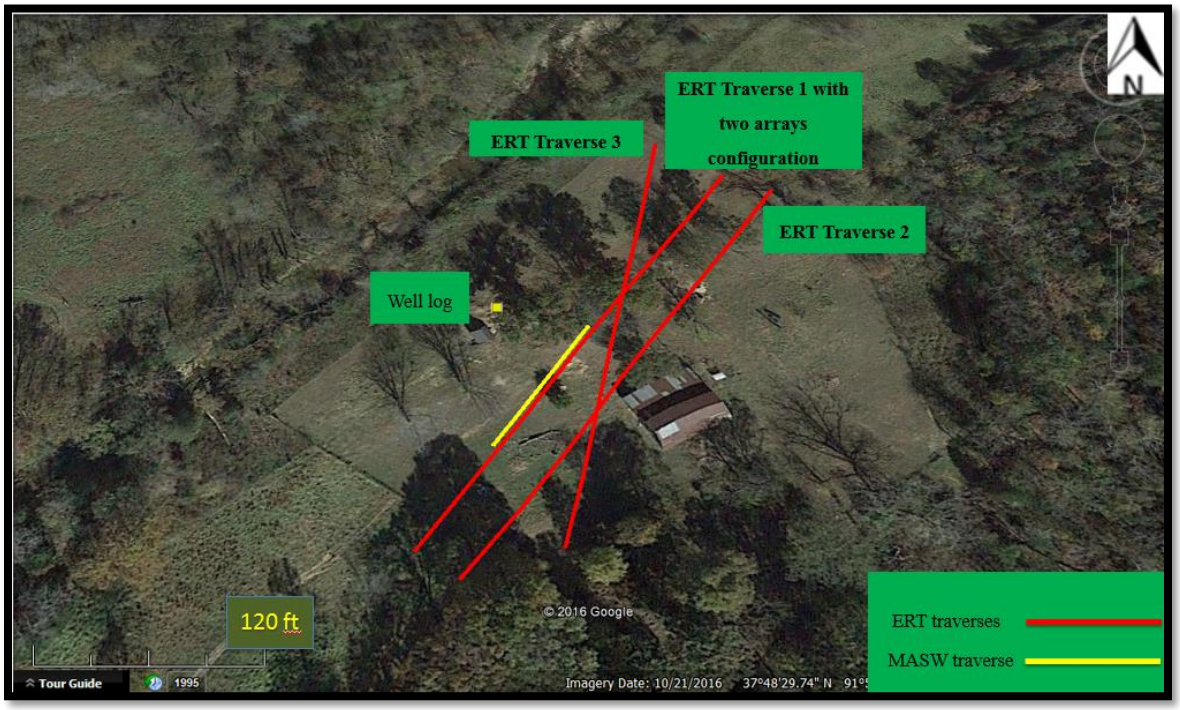

Figure 5.3. The approximate locations of the MASW and ERT traverses on the study area.

sledge hammer was utilized in this study as a source that impacted to the metal plate to generate waves that can be recorded by receivers (geophones) as a function of time (Figure 5.4a).

The triggering mechanism is required to signal the seismography and match the time with the arrival of the transmitted surface wave for impact sources. Figure 5.4b shows a simple triggering system attached to a sledgehammer.

The receiver (or geophone) are electromechanical transducers in direct contact with earth, which, is converted the motion of the earth producing from the shot into an electrical analog signal.

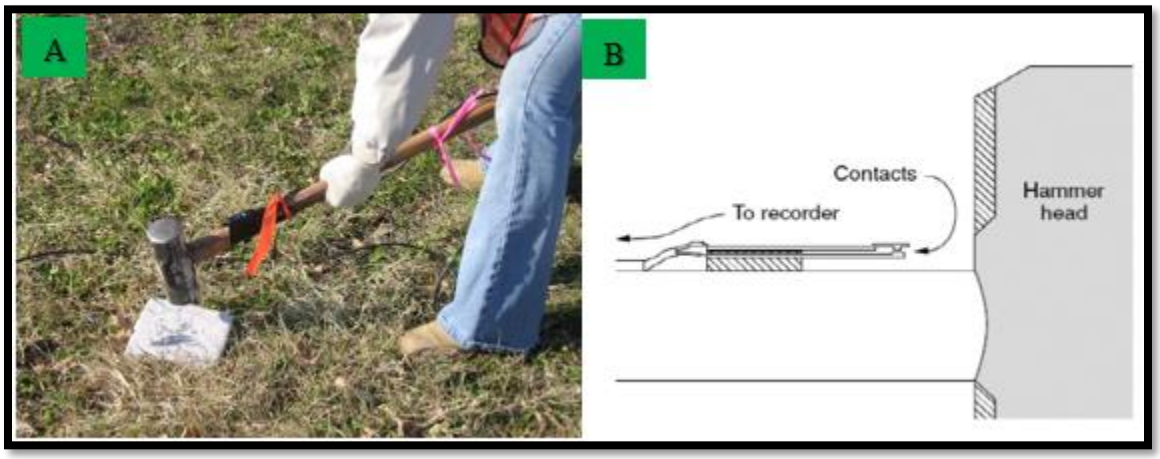

Figure 5.4. A seismic source, a) A 20lb. sledge hammer with metal plate, and b) Example of Sledgehammer Triggering Device (Milson, 1996).

A Seistronix RAS-24 Seismograph was utilized to conduct the MASW surveys. Seismographs are utilized to record and analyze the transmitted signal from the geophone into a visible trace or shot record (Milson, 1996). A common Windows laptop computer is used to control the 24 channel system. A typical 12V battery was used as a power source. Figure 5.5 illustrates the field setup of MASW.

Analog electrical impulses are travelled from the individual geophones to the seismograph through a cable system. The cable is metallic and transfers the signal with little resistance.

Figure 5.5. MASW field setup, a) seismograph, laptop and 12V battery and b) 4.5 Hz Geophones with spikes.

Figure 5.6 and 5.7 show an example of shot gather for each array configuration record at same source offset of 20ft with different geophone interval. The record illustrates that the surface waves (ground roll) have larger amplitudes than other waves such as refraction and reflection waves.

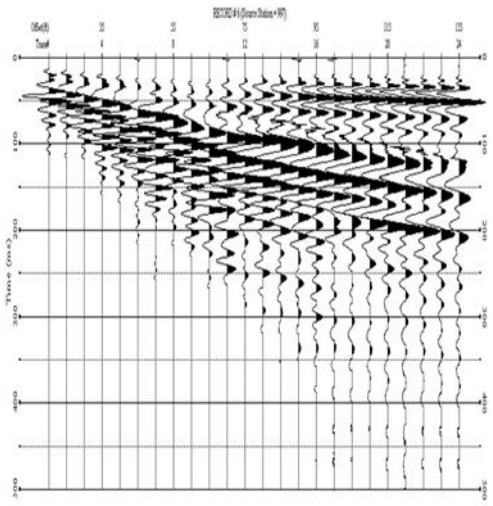

Figure 5.6. Raw seismic field record, with 20ft source offset and 5ft geophone interval.

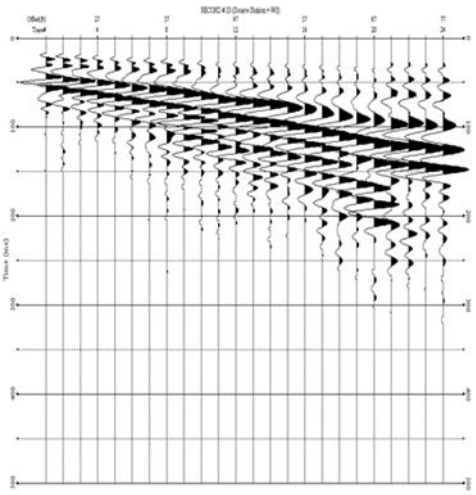

Figure 5.7. Raw seismic field record, with 20ft source offset and 2.5ft geophone interval.

5.2.2. Processing of MASW Data. The acquired data were downloaded and processed using Surfseis4 software developed by the Kansas Geophysical Survey (KGS). The processing of the data was successfully completed as explained in section three. Some pre-processing steps were applied on the raw seismic field record include (1) converting the field record format to the Kansas data processing format (2) muting undesirable signals of body waves like refracted and reflected signals that affect the resolution of multimodal dispersion curves and the accuracy of picking the dispersion curve. The muting step is discussed in the following section. (3) Analyzing the velocity and frequency to estimate the phase velocity of the surface waves.

The MASW data were fair to good quality and could not be processed before using the mute technique. After applying the mute technique to the acquired data of a short length configuration (array length is 57.5ft), the data were improved significantly and was able to pick an accurate dispersion curve. Therefore, the result of one-dimensional shear wave velocity profile was fairly acceptable. Conversely, the acquired data of a long length configuration (array length is 115ft) traverse was noisy and could not be processed, and therefore one-dimensional shear wave velocity profile of this data could not be generated. The reasons that prevent the data of a long length configuration from being processed will be discussed in section 6.

5.2.2.1. Muting. The objective of muting is to remove parts of seismic wave field such as the direct wave, refracted waves and higher modes of the surface wave that might act like noise and affect an extraction of reliable dispersion curve (Ivanov et al., 2001).

Generally, surface wave propagates in a number of modes, this might create several curves of various modes appearing in the dispersion property. The curve that has

the lowest value of velocity is called fundamental mode, and the other curves with higher values of velocity are called higher modes (1st, 2nd, etc.) based on their velocity values. Additionally, the curves of higher mode would appear with smaller slopes than the fundamental mode (Ivanov et al., 2001). In fact, the essential goal of muting is separating various wave fields to enhance dispersion curve picking. Figures 5.8 and 5.9 show the result of muting on the shot gather and the dispersion curves of profile1 with 20ft source offset and 2.5ft geophone interval.

One-dimensional shear-wave velocity profile was generated form the MASW traverse1, which represents the shear velocity at the mid-point of the array configuration (at station 170 ft. of traverse1 of ERT data). This profiles is shown in Figure 5.10.

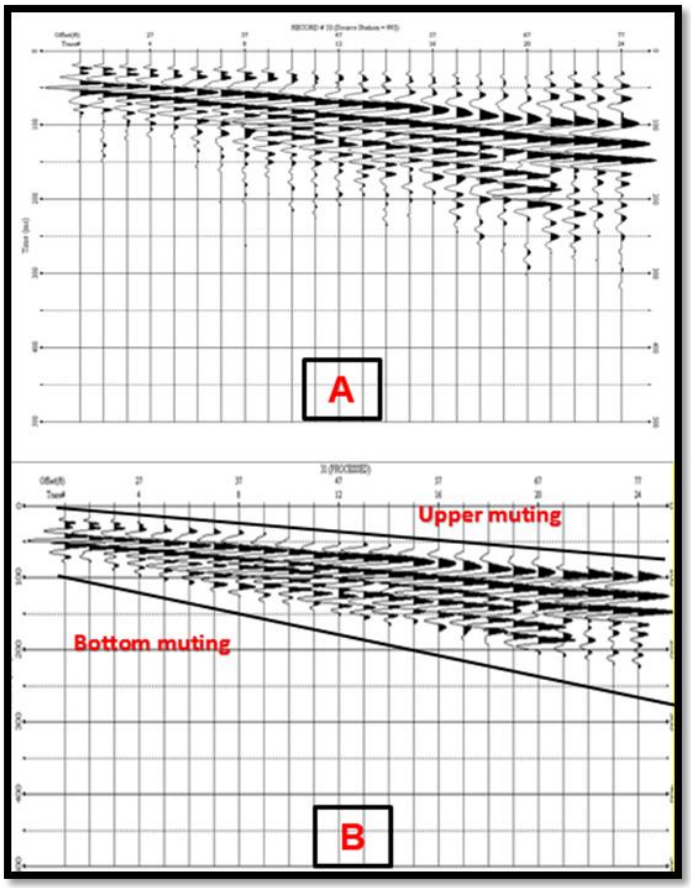

Figure 5.8. Raw seismic field record, with 20ft source offset and 2.5ft geophone interval. (A) Before muting and (B) after muting.

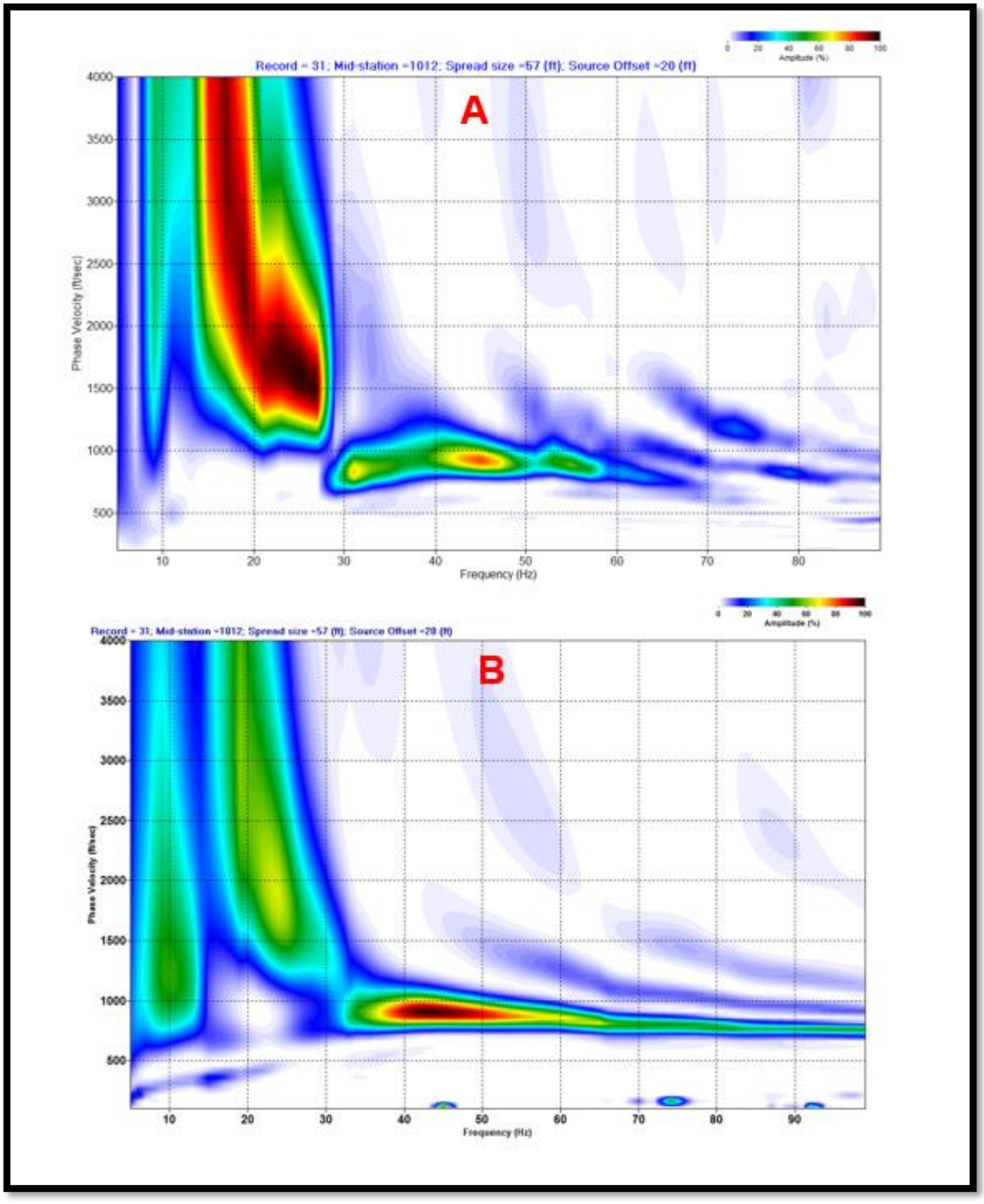

Figure 5.9. Dispersion curve for 20ft source offset and 2.5ft geophone interval (A) Before muting and (B) after muting.

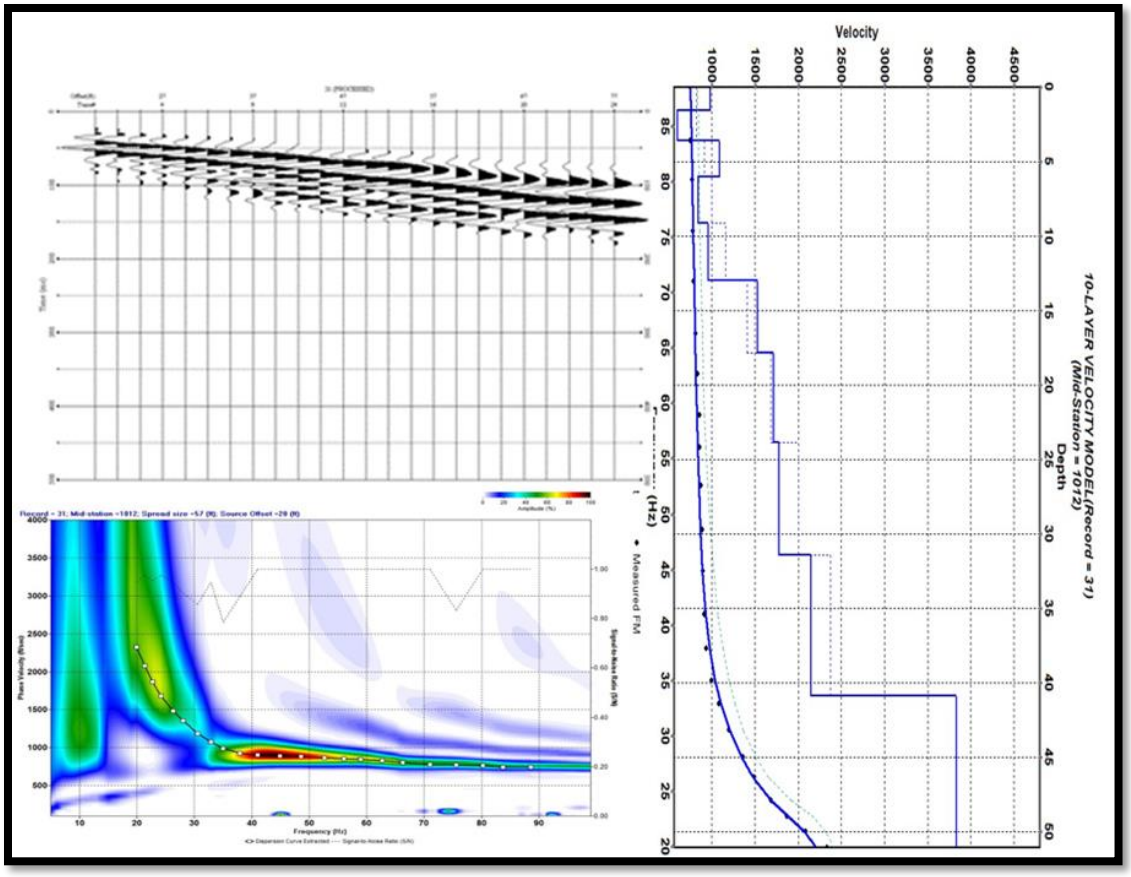

Figure 5.10. Raw seismic data, dispersion curve, and One-dimensional shear-wave velocity profile #1centered at station 170 ft. of traverse1 of ERT data.

5.3. THE ELECTRICAL RESISTIVITY TOMOGRAPHY (ERT) METHOD

5.3.1. Acquisition of ERT Data. Four electrical resistivity profiles were acquired on the surface along three traverses (Traverses 1, 2, and 3, Figure 5.11). The main purpose of the measurements was to map the subsurface in the study area to a depth of 70ft, and to compare two different arrays of (ERT) method, namely dipole-dipole array and Wenner-Schlumberger. The second purpose was to compare the ERT-estimated depth to top-of-rock and the MASW-generated depth to top-of-rock.

The four ERT profiles were recorded using an AGI SuperSting R8/IP resistivity unit equipped with eighty-four 84 electrodes at five feet spacing. The length of each

profile was 415 feet. The estimate depth of investigation was about 70 ft. The traverses 1 and 2 were oriented SW–NE, whereas a Traverse 3 was directed S-N crossing the other two traverses as seen in Figure 5.11. Traverse1 was acquired with two different array configurations, namely Wenner-Schlumberger array and dipole-dipole arrays, while the other two traverses were acquired with only dipole-dipole array configuration.

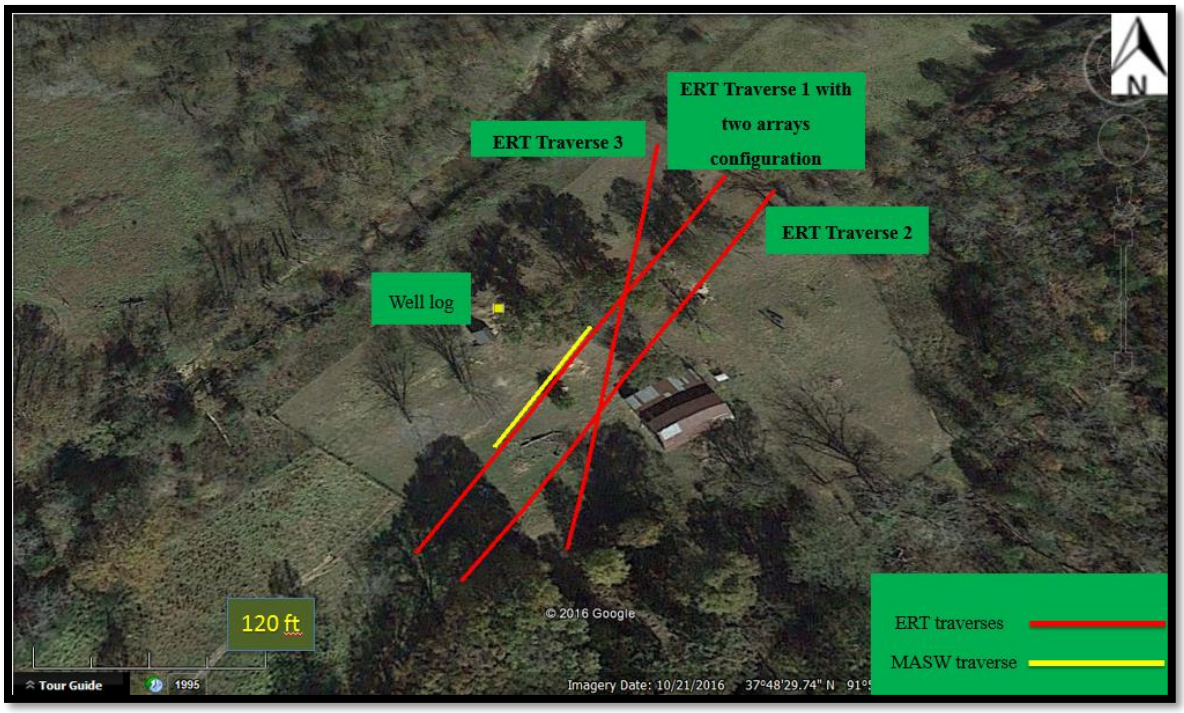

Figure 5.11. Map of the study area from Google shows the approximate locations of the ERT traverses and a well log.

5.3.1.1. Equipment used for ERT. A Multi-channel portable memory earth resistivity meter-SuperSting R8/IP (Figure 5.12). SuperSting system is an automated unit that measures the apparent resistivity of the subsurface. Two 12 volt battery were used in this project to power the SuperSting R8/IP.

Eighty-four (84) electrodes were connected to the insulated low resistance multi-core cable with an equal amount of metal stakes. These electrodes are connected to the

switching unit that connects the SuperSting as well. Additionally, the SuperSting is connected to a laptop computer which is used to store data.

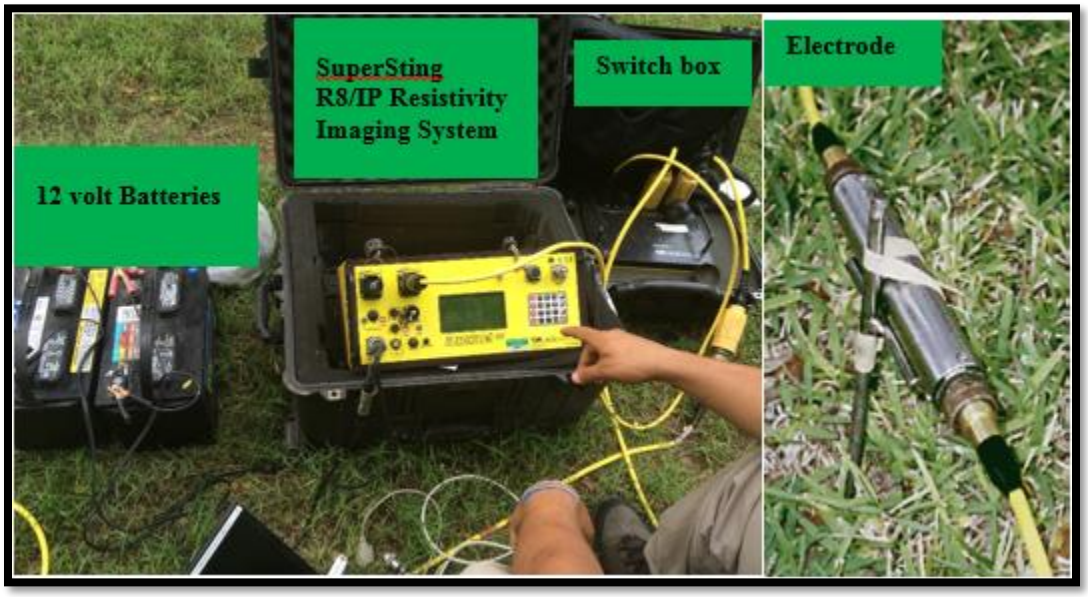

Figure 5.12. The equipment of ERT for data acquisition.

5.3.2. Processing of ERT Data. The acquired data were processed using RES2DINV software with applying the same processing steps discussed in chapter 4 to generate a 2D resistivity model of the subsurface materials. Figures 5.13 5.14, 5.15, and 5.16 illustrate the generated models as uninterested profiles.

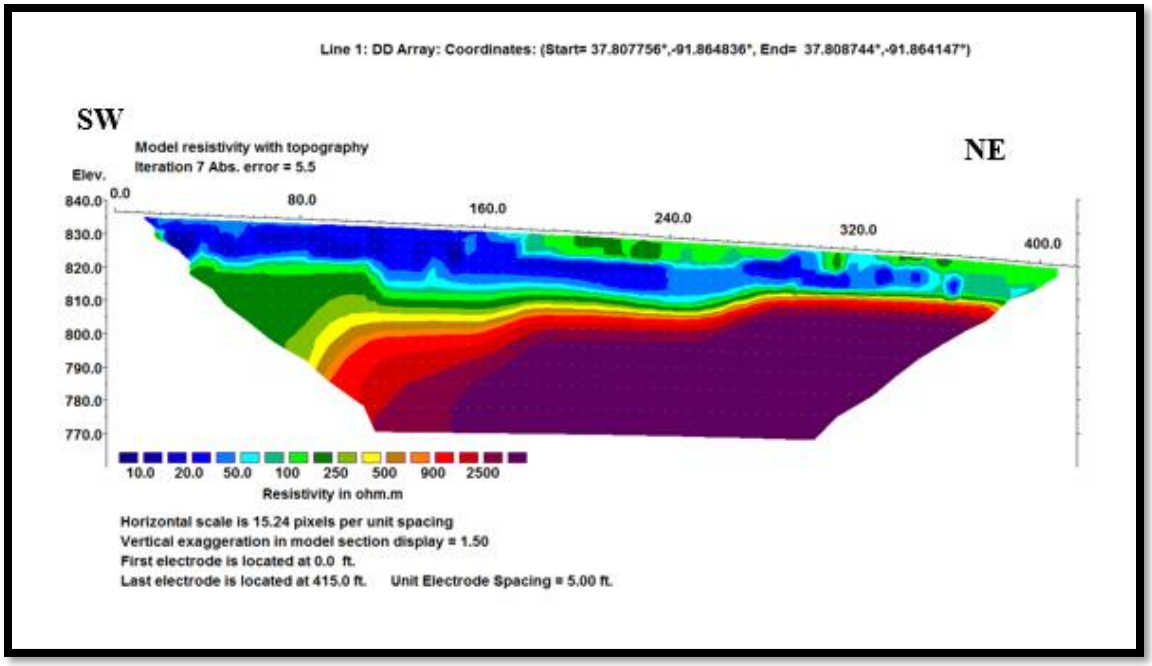

Figure 5.13. Uninterpreted ERT Profile 1, oriented southeast-northwest along a 415-ft traverse 1 with dipole-dipole arrays configuration.

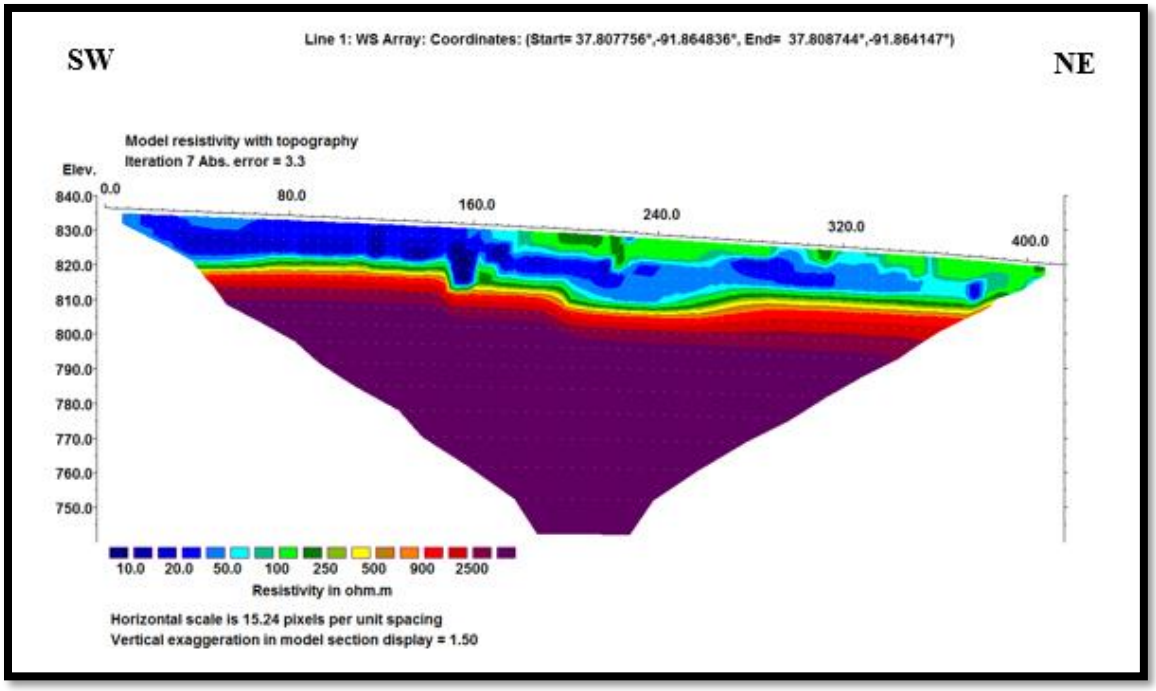

Figure 5.14. Uninterpreted ERT Profile 2, oriented southeast-northwest along a415-ft traverse 1 with Wenner-Schlumberger array configuration.

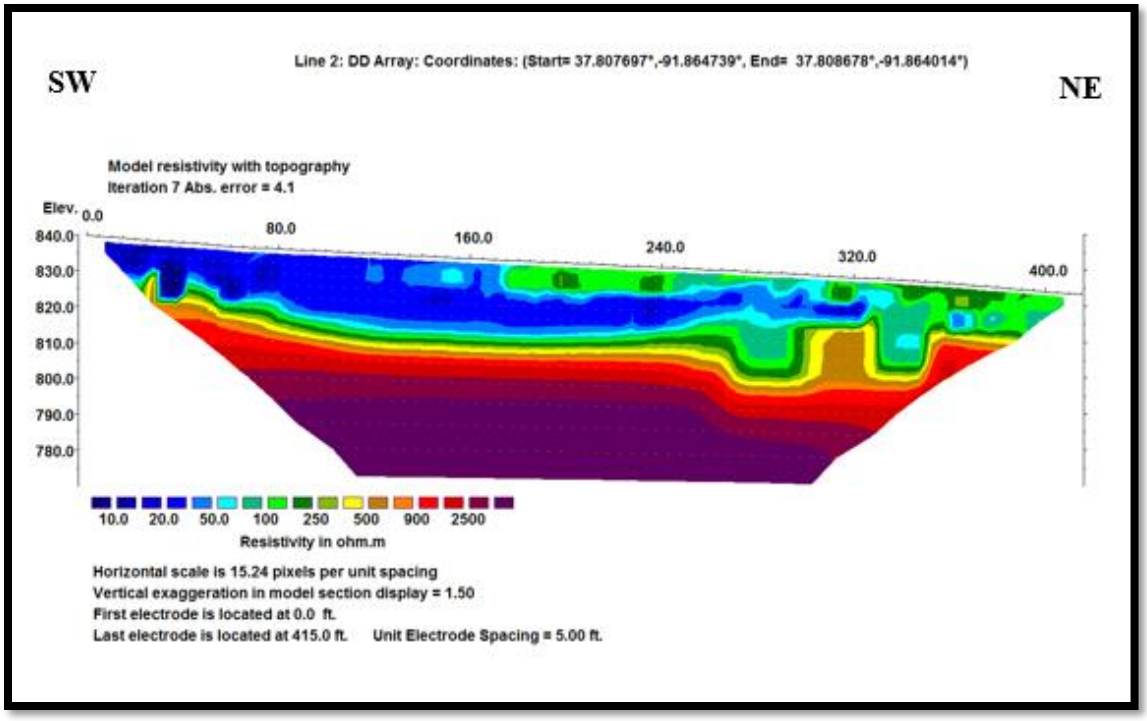

Figure 5.15. Uninterpreted ERT Profile 3, oriented southeast-northwest along a415-ft traverse 2 with dipole-dipole arrays configuration.

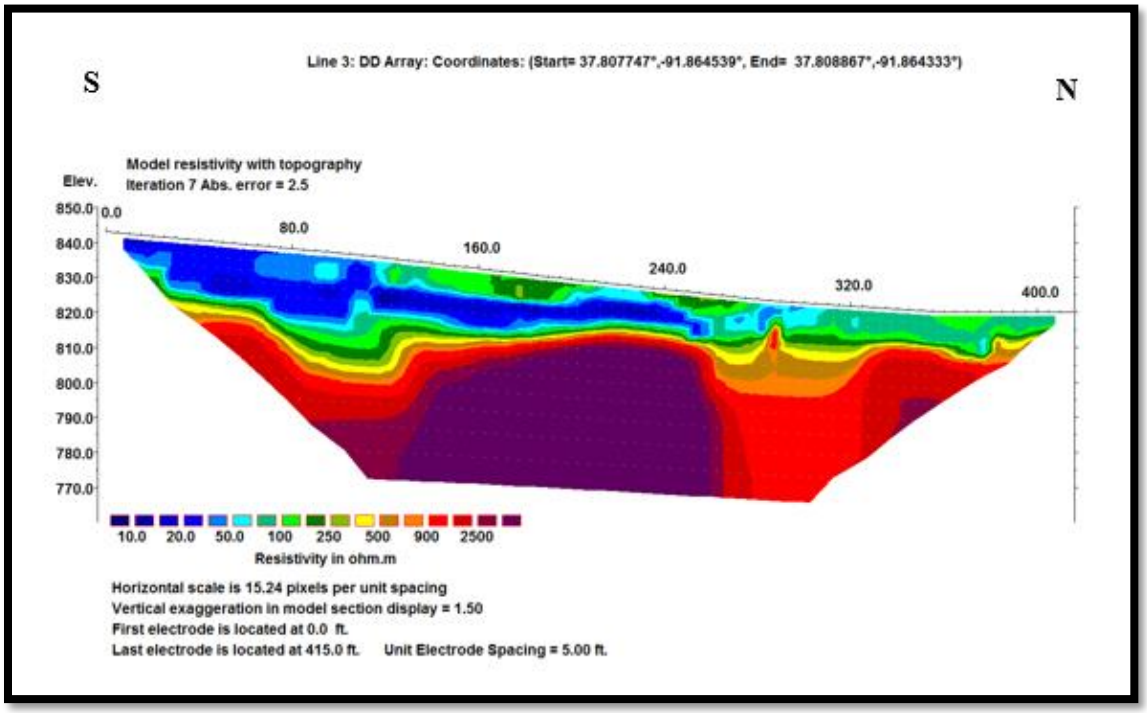

Figure 5.16. Uninterpreted ERT Profile 4, oriented south-north along a415-ft traverse 3 with dipole-dipole arrays configuration.

6. RESULT AND DISCUSSION

6.1. MASW DATA INTERPRETATION

The acquired data of a long length configuration (array length is 115ft) was noisy and could not be processed. The poor quality of this data is attributed smearing that could be caused by the complex stratigraphic of the subsurface as indicated by the ERT images. In this case, it is difficult to differentiate between the fundamental mode and the higher mode energy. Picking the dispersion curve would lead to an inaccurate estimation of shear wave velocity and depth investigation.

The recorded surface wave data obtained from this data from both ends of array spread with 30ft source offset showed that there are two velocity slopes of surface waves (Figure 6.1 and 6.2). And an extracting dispersion curve of this field record showed that dispersion curve image patterns vary at low and high-frequency ranges. Figure 6.1 and 6.2 show two examples of the acquired data of a long length configuration (array length is 115ft).

Additionally, there is a dip associated with the subsurface layers under the survey of this data. Shooting direction of this survey was updip. This was indicated by the slope of surface waves (Figure 6.1), which was appeared as a straight line, but as it moves updip the slope changed and had less distance to travel to the surface with a different velocity. This was also indicated by the Wenner-Schlumberger ERT image that shows that the subsurface layers are not horizontal and they are updip, in which the start of MASW survey that centered at 200ft mark on Wenner-Schlumberger ERT profile and oriented northwest- southeast.

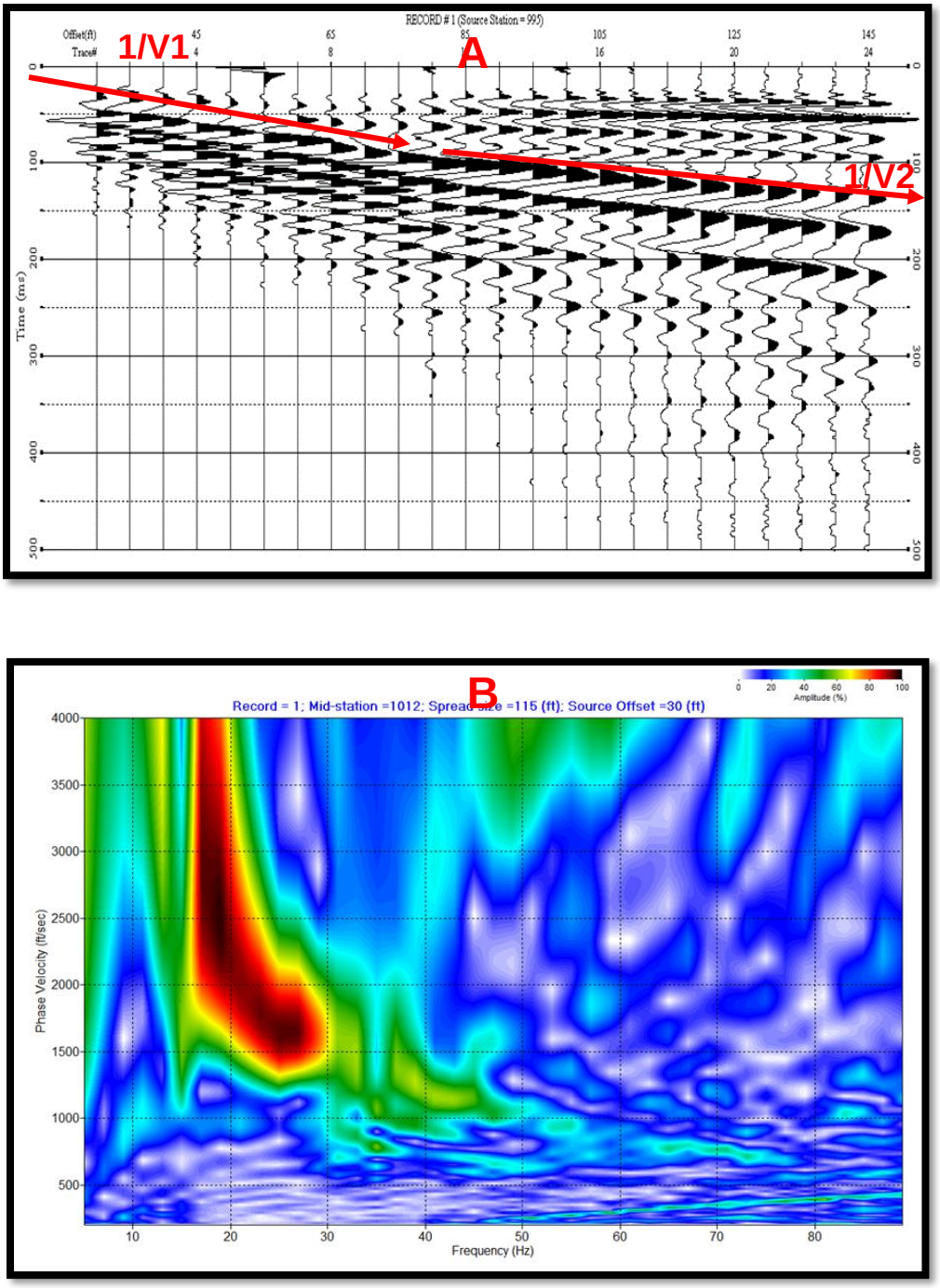

Figure 6.1. (A) Raw seismic field record from NE to NE direction (B) an extracting dispersion curve of 30ft source offset and 5ft geophone interval. Red lines represent the velocity trend.

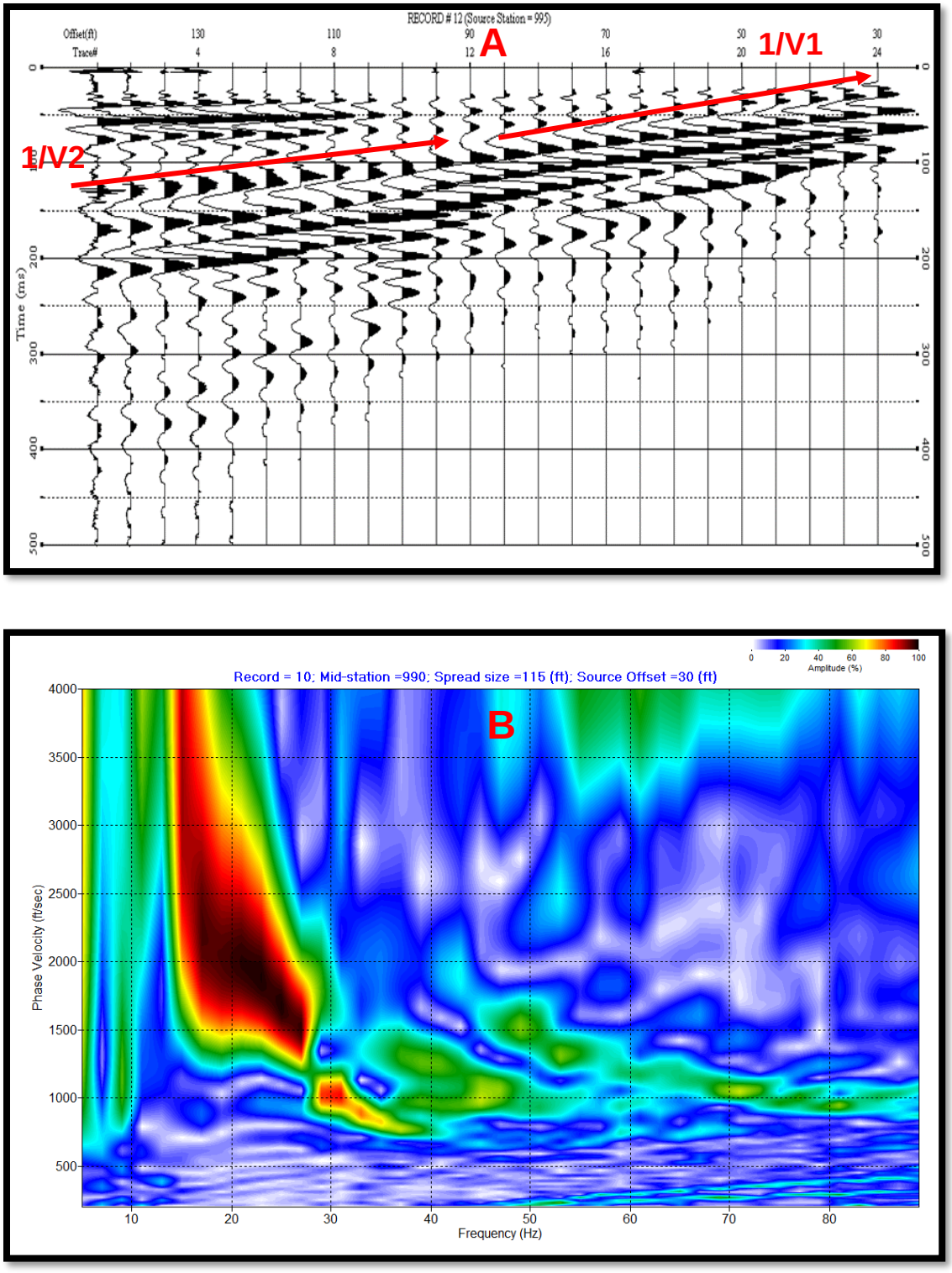

Figure 6.2. (A) Raw seismic field record from NE to SW direction (B) an extracting dispersion curve of 30ft source offset and 5ft geophone interval.

For the interpretation result of MASW1 data that has a short spread (array length is 57.5 ft.), the depth to the top of rock from MASW1 profile centered at 170 feet mark on ERT profile 1 and 2 was mapped at 13ft with MASW shear-wave velocity of 1,500 ft/s. This depth correlates well with the mapped depths to the top of bedrock in (ERT) profile2 that had Wenner-Schlumberger array configuration. However, the mapped depths to the top of bedrock in (ERT) profile1 with dipole-dipole arrays configuration was not correlate well with the multichannel analysis of surface waves one-dimensional shear wave velocity. Mapped depth to the top of bedrock using ERT was determined using 70 Ohm-m contour Interval.

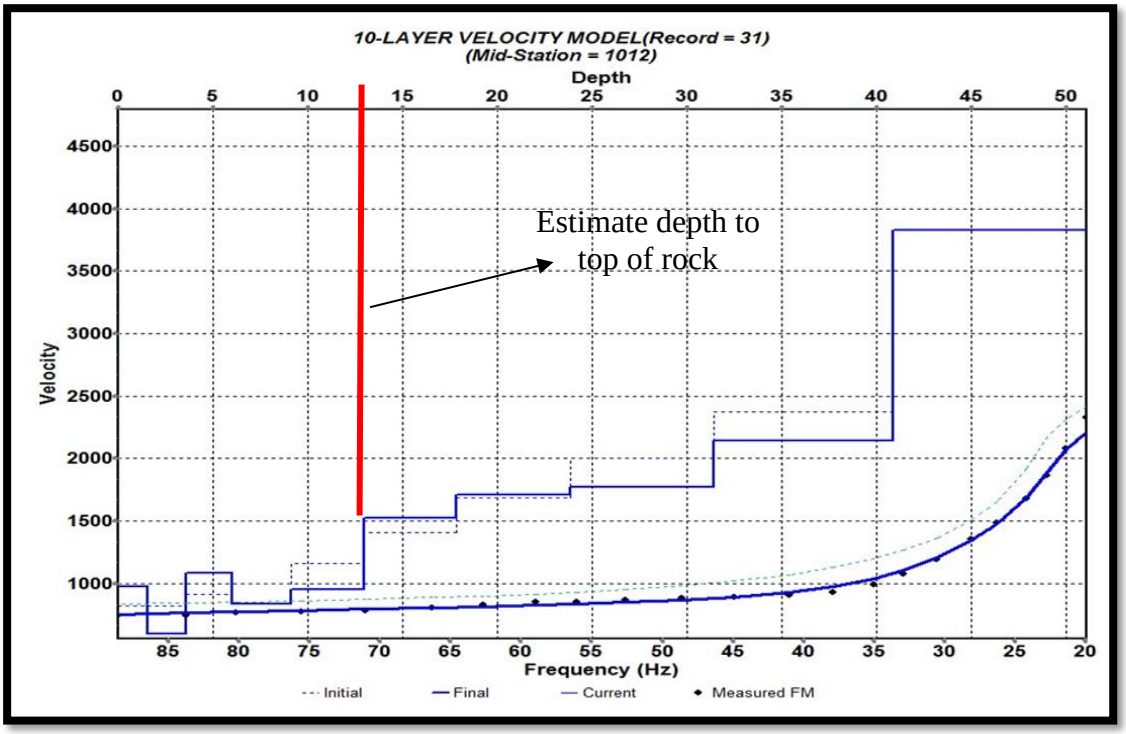

Figure 6.3. One-dimensional shear wave velocity profile centered at 170 feet mark on ERT profile 1 and 2. Interpreted depth to top of rock was 13ft for the MASW data, while around12 feet on ERT profile2 with Wenner-Schlumberger array configuration and 16 feet on ERT profile1 with dipole-dipole arrays configuration. This means that Wenner-Schlumberger array configuration correlates well with MASW result of depth to top of rock.

6.2. ERT DATA INTERPRETATION

There are several factors such as porosity, conductivity, temperature, salinity, clay content, saturation and lithology can impact the resistivity of earth materials. Variation in the resistivity of the subsurface mainly represents the different materials of the subsurface. Therefore, the interpretation of the ERT data is based on the resistivity values of earth materials such as limestone, dolomite, sand, and clay. The resistivity values of the most common earth materials were discussed in chapter 4.

Additionally, the knowledge of the general resistivity values of common subsurface conditions such as moist clay, moist soils and highly fractured rocks, relatively intact limestone and air-filled cavities are crucial for interpreting the ERT data. Table 6.1 describes the general resistivity values of these materials.

The four processed ERT data were interpreted (Figures 6.4, 6.5, 6.6 and 6.7) depending on the resistivity values, the one-dimensional shear wave velocity profile centered at 170 feet mark on traverse1 and available borehole logs for ground truth. The estimate depth to the bedrock was mapped based on the MASW interpretation and characterized by resistivity values equal to or in excess of 70 ohm-m with thickness ranging from 7 feet to around 22 feet. As a result, the resistivity contour value of 70 ohm-m is used as the top to the bedrock on all of the other ERT profiles. This value is usually for limestone and was supported by well log data of well#00418894 that describe the subsurface layer from 5ft to 80ft as limestone. This well is located about 60ft away from the ERT Traverse1. However, the depth to bedrock from the nearest well logs to the study area was ranging from 20 feet to around 30 feet (Figure 6.8).

Table 6.1. Describes the general resistivity values of common subsurface materials (Nwokebuihe, 2014).

Subsurface Material	**Description**	**Resistivity (Ohm.m)**
Moist Clays	Very low resistivity and varies based on its degree of saturation, porosity and layer thickness	< 100
Moist soils and intensely fractured rocks	Moderate resistivity and could vary based on its degree of saturation, porosity and layer thickness	100-400
Relatively Intact rock	Slightly higher resistivity and could vary based on its degree of saturation, porosity and layer thickness	> 400
Air-filled cavities	Very high resistivity and could vary depending on the conductivity of the surrounding strata and the depth/size/shape of void.	Usually >10,000

6**.2.1. Side-by-Side Comparison of All ERT Profiles with Dipole-Dipole Arrays**. A side-by-side comparison of the dipole-dipole Arrays is shown in Figure 6.9. Generally, the resistivity increases with the depth along the three profiles. At the study area, weathered rock characterized by values between 250 and 1500 ohm-m and intact/dry rock is by resistivity values in excess of 1500 ohm-m and.

Most of the resistivity contour value of 20 ohm-m or less were interpreted as moist clay soils, whereas the resistivities with contour values range from 100 ohm-m to 400 were interpreted as transitional zones consisting of either dry soil or fractured.

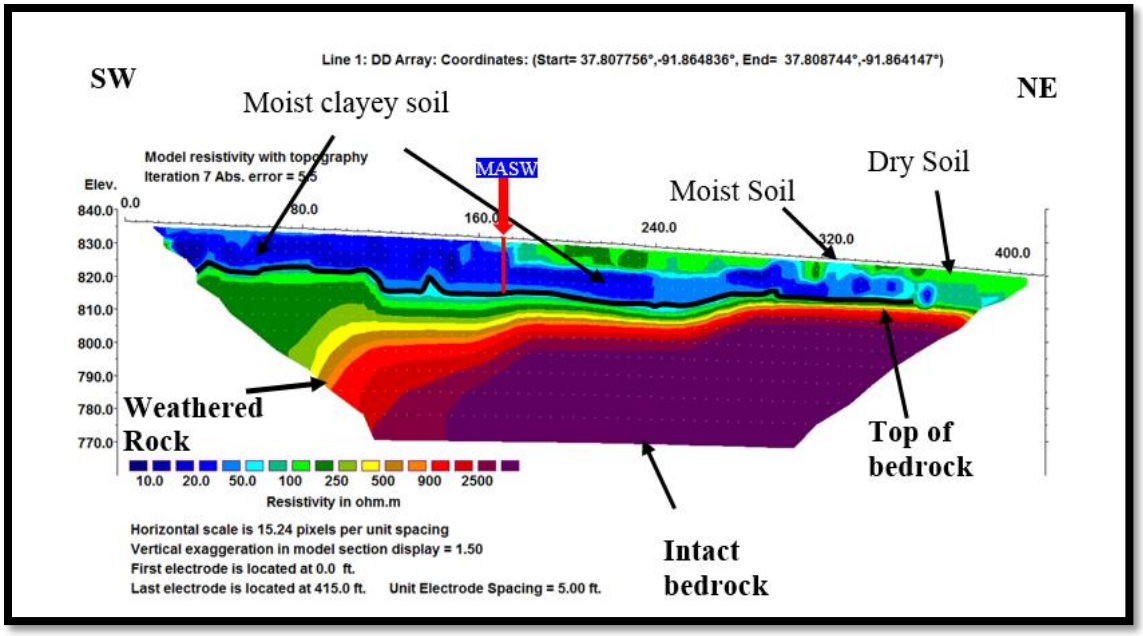

Figure 6.4. The interpretation of ERT Profile 1, oriented southeast-northwest along a415-ft traverse 1 with dipole-dipole arrays configuration. Black line represents top of bedrock that is picked at the top of the light blue contour. The red lines represent the location of the 1-D shear wave velocity profiles.

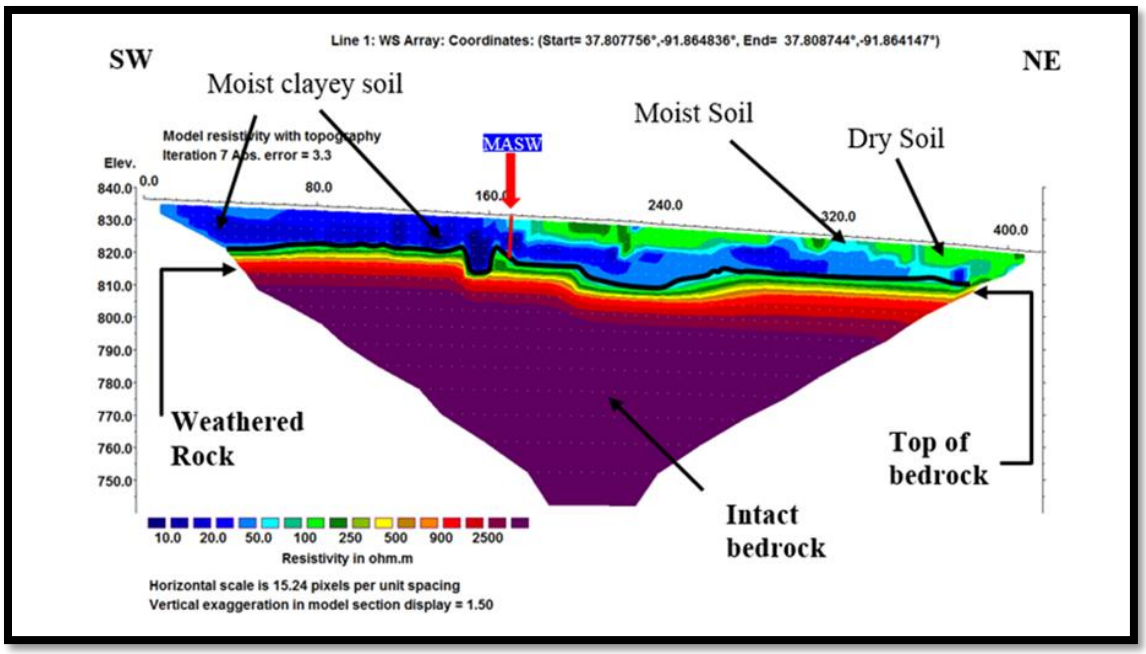

Figure 6.5. The interpretation of ERT Profile 2, oriented southeast-northwest along a415-ft traverse 1 with Wenner-Schlumberger array configuration. Black line represents top of bedrock that is picked at the top of the light blue contour. The red lines represent the location of the 1-D shear wave velocity profiles.

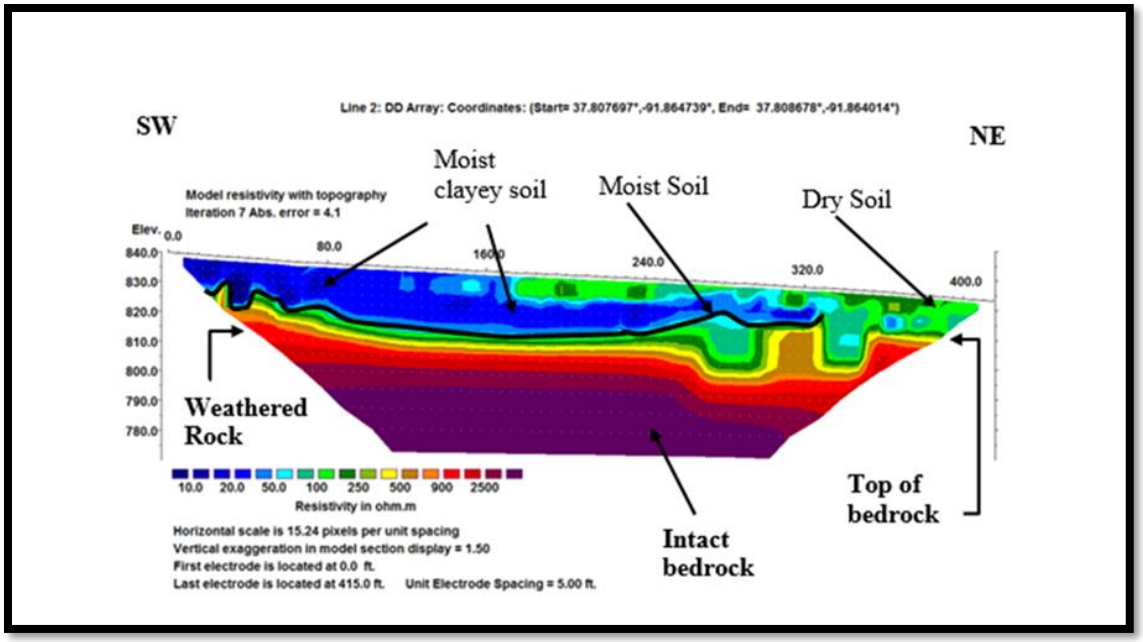

Figure 6.6. The interpretation of ERT Profile 3, oriented southeast-northwest along a415-ft traverse 2 with dipole-dipole arrays configuration. Black line represents top of bedrock that is picked at the top of the light blue contour.

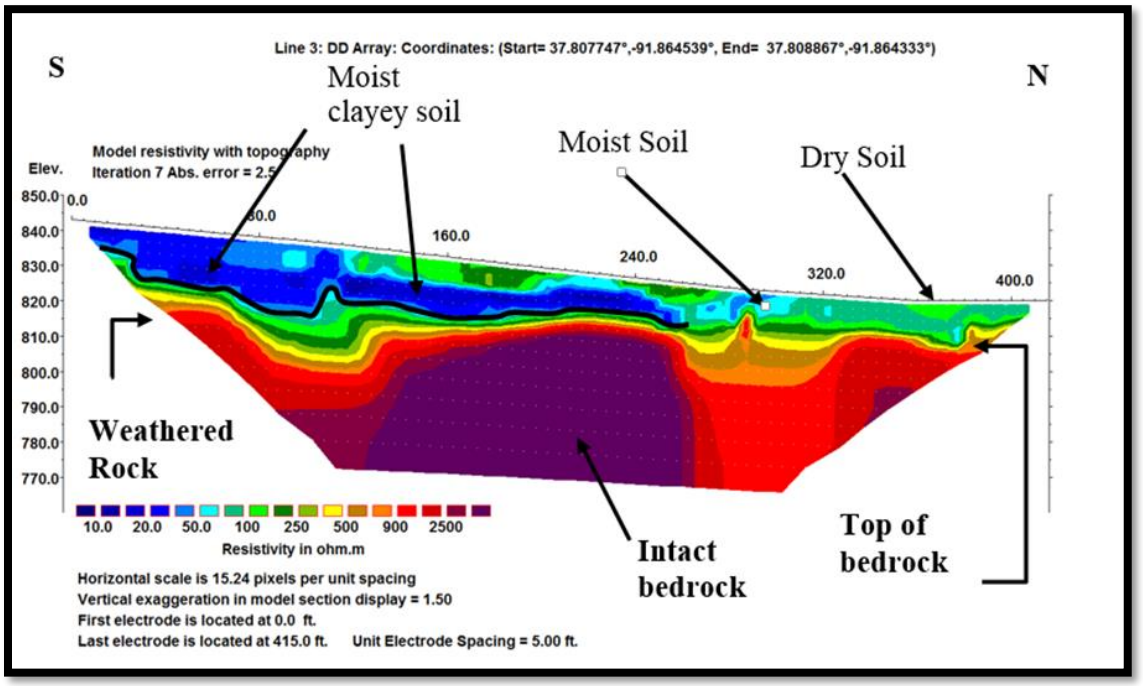

Figure 6.7. The interpretation of ERT Profile 4, oriented south-north along a415-ft traverse 3 with dipole-dipole arrays configuration. Black line represents top of bedrock that is picked at the top of the light blue contour.

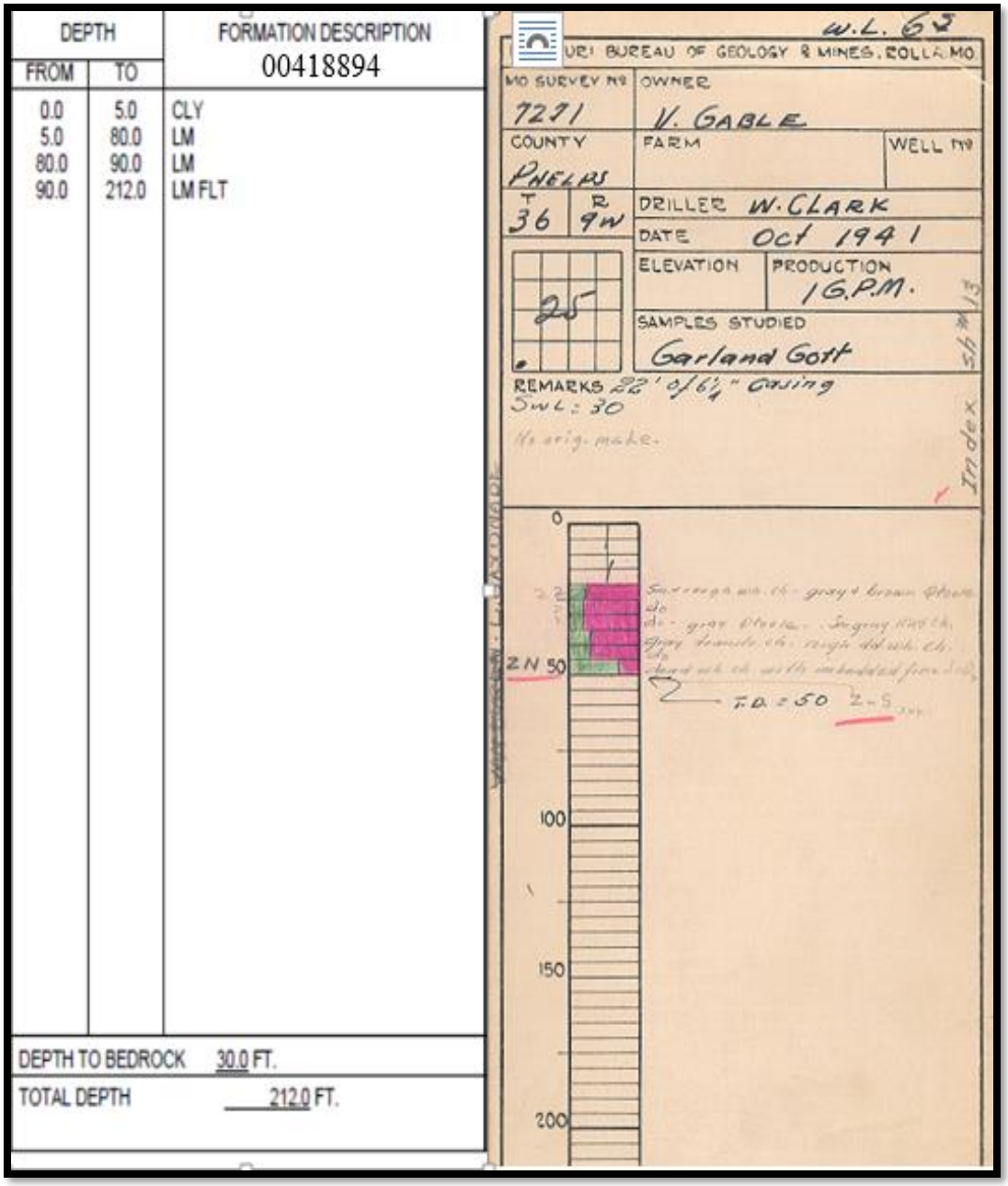

Figure 6.8. Well logs 00418894 and 007271 (Missouri Department of Natural Resources).

There is a large resistive region with a resistivity value range from 10 ohm-m to 20 from the southwest start of the traverses up to a horizontal station of about a 320 feet at the three traverses. This law resistive area interpreted as moist clays, underlain by dry soil, weathered rock, and intact rock.

6.2.2. The Comparison between Wenner-Schlumberger and Dipole-Dipole Arrays of ERT. A side-by-side comparison of the two different arrays of ERT method (Wenner-Schlumberger Array and dipole-dipole Arrays) that were acquired on ERT Traverse1 is shown in Figure 6.10.

Generally, the horizontal data coverage of Wenner-Schlumberger is narrower than the horizontal data coverage of with the dipole-dipole array. Most sections on both ERT profiles that are interpreted based on different subsurface materials are correlated well as shown in Figure 6.9 except two zones that show a different feature for each array.

First, at a horizontal station of about a 170 feet where the MASW is located, the Wenner-Schlumberger Array profile shows a small low resistivity anomaly that eroded a section of the weathered boundaries that have a resistivity value started from about 250 ohm-m. On the other hand, the dipole-dipole array profile does not show this small feature. This means that the Wenner-Schlumberger Array can image the shallow vertical structure superior to the dipole-dipole Array.

Second, in the southwest part of Traverse1 at depth of about 18 to 48ft, the dipole-dipole Array profile shows a high resolution of horizontal weathered boundaries that have resistivity contour values between 150 and 2000 ohm-m. However, the Wenner-Schlumberger Array profile shows this part with thin weathered layers at thickness of 8ft with same resistivity values, underline by intact rock. In fact, the dipole-dipole Array is sensible of horizontal variation of the resistivity value.

For the depth to the bedrock compared with the MASW method result, the depth to the top of rock from MASW1 profile centered at 170ft mark on ERT Traverse1 was mapped at 13ft. This depth correlates well with the Wenner-Schlumberger array profile that mapped depth to top of bedrock at 12ft in the same location. However, the dipole-

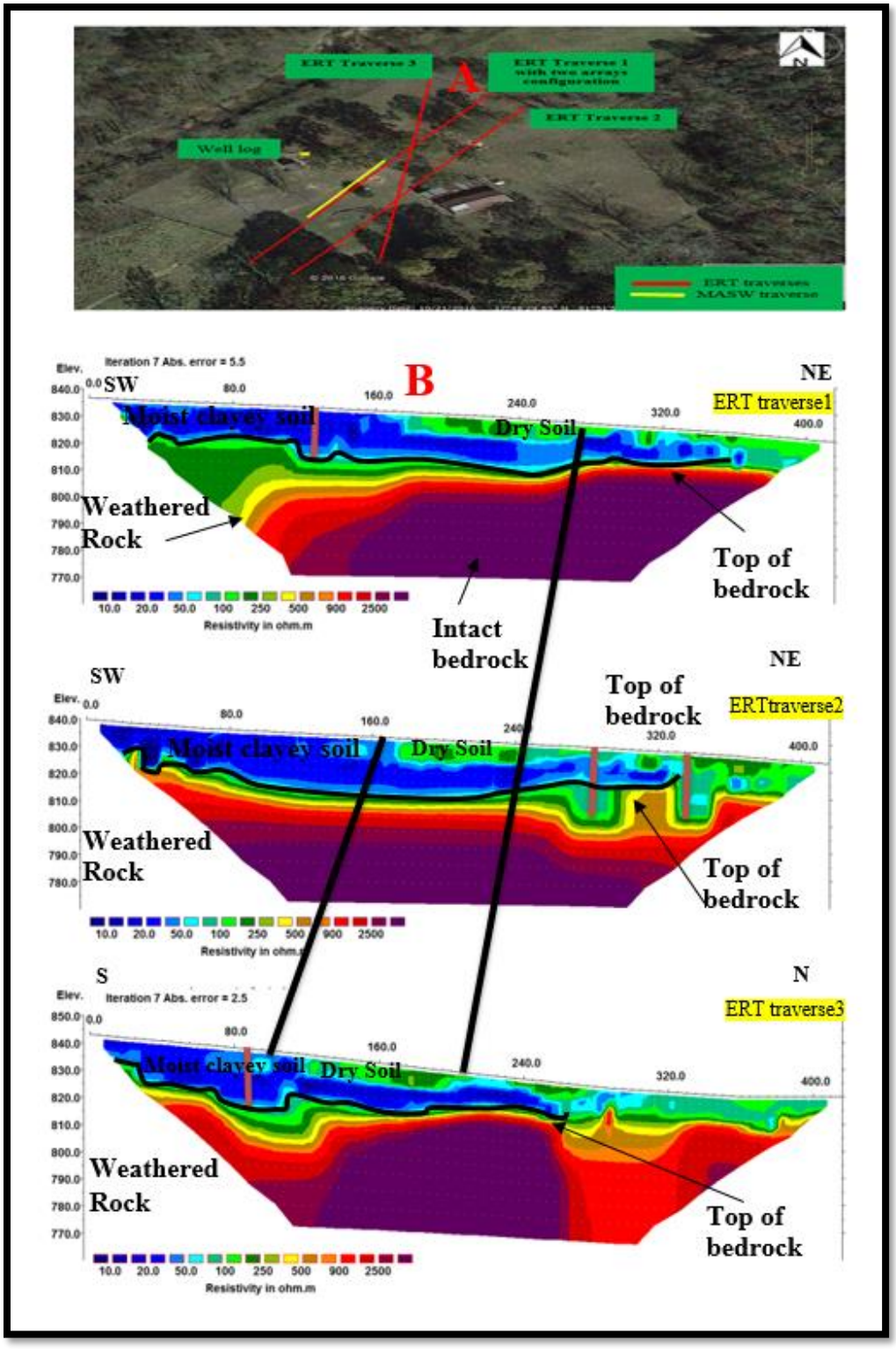

Figure 6.9. (A) The approximate locations of the ERT traverses and a well log. (B) Side-by-Side Comparison of All ERT Profiles with dipole-dipole Arrays. The two parallel black lines represent the cross points between Profile 4 and the other two profiles. Blue lines represent anomalies.

dipole arrays profile mapped depth to top of bedrock at 16ft in the same location, which is slightly less correlated with the MASW1 result, but the dipole-dipole data appear to better image limestone bedrock regarding lateral resolution as shown in Figure 6.11.

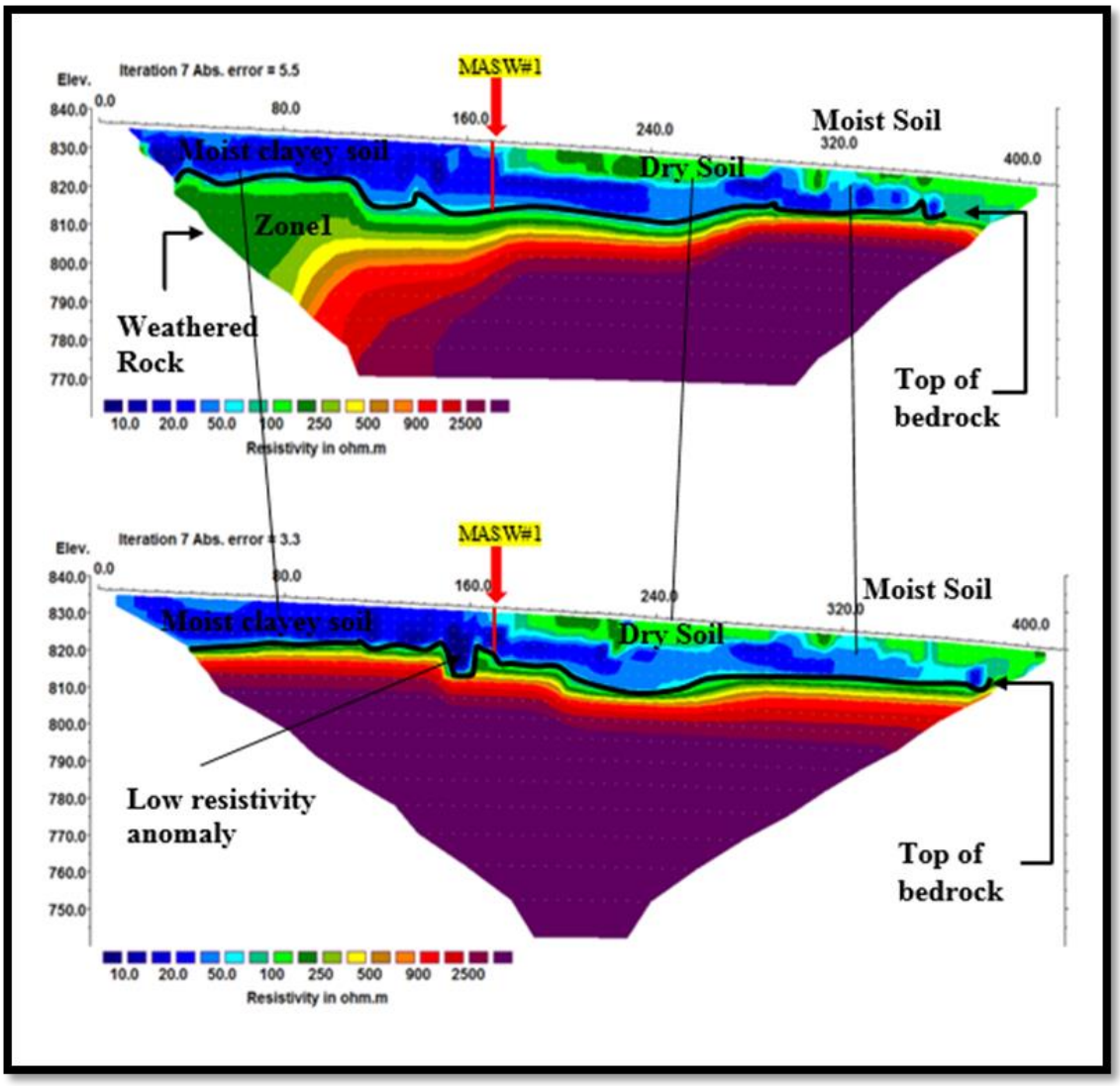

Figure 6.10. The Comparison between (A) dipole-dipole arrays and (B) Wenner-Schlumberger array and of ERT. Profiles A and B are oriented southeast-northwest along a415-ft traverse 1. Black line represents top of bedrock that is picked at the top of the light blue contour. The red lines represent the location of the 1-D shear wave velocity profiles.

Figure 6.11 shows MASW1 tied to the ERT profile1 at 170ft mark. The dipole-dipole image of profile1 indicates a lateral resolution to the weathered rock zone that has resistivity contour values between 150 and 2000 ohm-m at depth of about 16 to 40ft lateral resolution. This is characterized by a shear wave velocity ranging from 1500ft/sec to 3800ft/sec. This range of shear wave velocity is consistent with soft rock and rock.

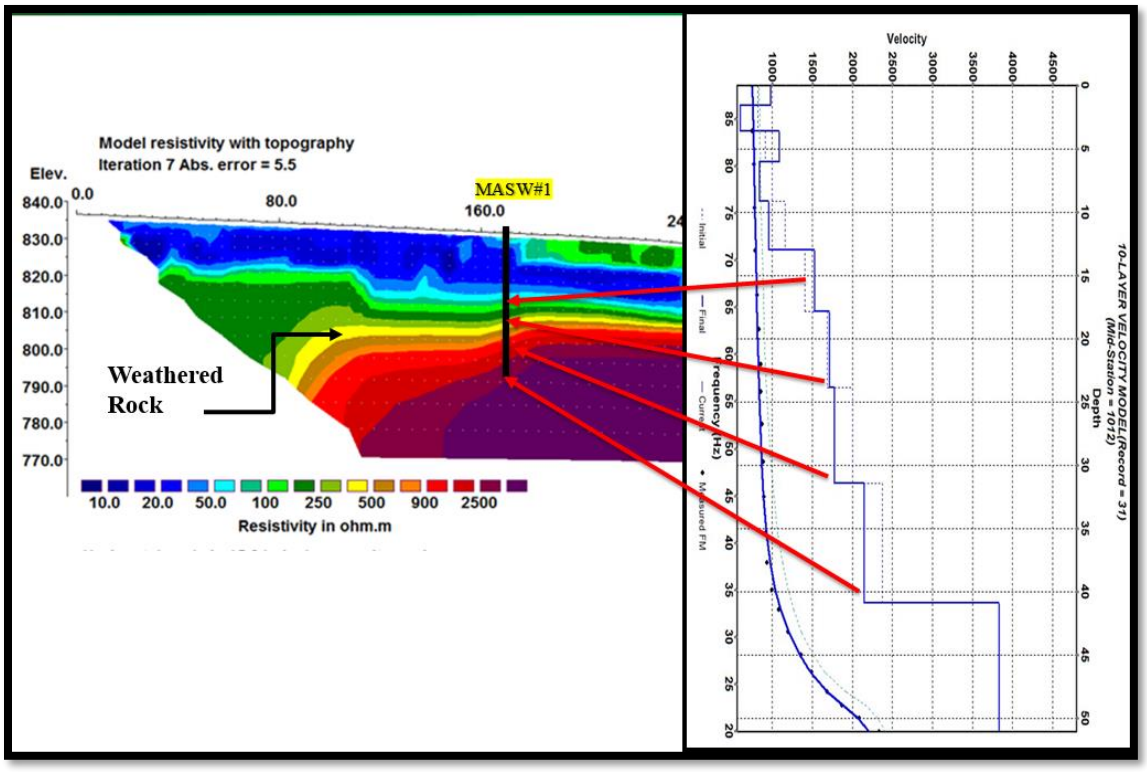

Figure 6.11**.** Correlation of the interpretation of (ERT) profile1 with dipole-dipole arrays configuration and shear wave velocity profile of MASW1.

7. CONCLUSIONS

The primary objectives of this research were to image the subsurface in the study area to a depth of 70 feet and to compare the ERT images generated using both the dipole-dipole and Wenner-Schlumberger arrays. Secondary objectives were (1) to evaluate how variations in the MASW array configuration affected MASW data quality, and (2) to compare the ERT-estimated depth to top-of-rock and the MASW-generated depth to top-of-rock.

The ERT tool was used to image the subsurface in the study area. Soils were imaged and categorized as either dry, moist or moist clayey. Limestone bedrock was also imaged and categorized as weathered or intact.

The top-of-rock, as per the ERT interpretations, was consistent with the MASW-estimated depths to top-of-rock. The interpreted top-of-rock on the ERT profiles correlated well with the 70 ohm-m contour value. The top-of-rock on the MASW 1-D shear-wave data was mapped at 13ft with shear-wave velocity of 1,500 ft/s. These interpretations are consistent with available borehole control and published literature.

Depend on the comparative analyses of the dipole-dipole ERT data, the Wenner-Schlumberger ERT data, and MASW 1-D shear-wave data, it is concluded that the Wenner-Schlumberger ERT data are slightly more consistent with the MASW data in terms of depth to top-of-rock and determining dip direction of subsurface layers. However, the dipole-dipole data has a higher lateral resolution of limestone bedrock. Based on the analyses of the MASW data, it is concluded that better results were obtained using a 2.5-foot geophone spacing as opposed to a 5-foot spacing, probably because depth to top-of-rock varies significantly in places in the study area.

BIBLIOGRAPHY

Bormann, P., Engdahl, B., & Kind, R. (1999). Seismic Wave Propagation and Earth models. *Earth*, 1–70. https://doi.org/http://doi.org/10.2312/GFZ.NMSOP-2_ch2.

Burger, H. R., Sheehan, A. F., and Jones, C. H. (2006). *Introduction to Applied Geophysics: Exploring the Shallow Subsurface*. New York: W.W. Norton.

Chalikakis, K., Plagnes, V., Guerin, R., Valois, R., & Bosch, F. P. (2011). Contribution of geophysical methods to karst-system exploration: An overview. *Hydrogeology Journal*, *19*(6), 1169–1180. https://doi.org/10.1007/s10040-011-0746-x.

Everett, M. E. (2013). *Near-Surface Applied Geophysics*.

Ivanov, J., Park, C. B., Miller, R. D., Xia, J., & Overton, R. (2001). Modal separation before dispersion curve extraction by MASW method. *Symposium on the Application of Geophysics to Engineering and Environmental Problems 2001*, SSM3-SSM3. https://doi.org/10.4133/1.2922952.

Loke, D. M. (1999). Electrical imaging surveys for environmental and engineering studies. *Cangkat Minden Lorong*, *6574525*(1999), 63.

Loke, M. H. (2001). Tutorial : 2-D and 3-D electrical imaging surveys By, (March).

Nwafor, U. C. (2015). Optimum acquisition and processing parameters for multichannel analysis of surface waves using 3D electrical resistivity tomography as control.

Nwokebuihe, S. C. (2014). The description of an effective sinkhole investigation approach: A case study of two sites in Greene County, Missouri. *Ph.D. Thesis*.

Ólafsdóttir, E. Á. (2014). Multichannel Analysis of Surface Waves Methods for dispersion analysis of surface wave data, (December).

Park, C. B., Miller, R. D., & Miura, H. (2002). Optimum field parameters of an MASW survey. *Proceedings of the Society of Exploration Geophysicists (SEG) Japan Tokyo*, 22–23.

Park, C. B., Miller, R. D., & Xia, J. (1998). Imaging dispersion curves of surface waves on multi-channel record. *SEG Expanded Abstracts*, *17*(1), 1377–1380. https://doi.org/10.1190/1.1820161.

Park, C. B., Miller, R. D., & Xia, J. (1999). Multichannel analysis of surface waves. *Geophysics*, *64*(3), 800–808. https://doi.org/10.1190/1.1444590.

Park, C. B., Miller, R. D., Xia, J., & Ivanov, J. (2001). Seismic Characterization of Geotechnical Sites By Multichannel Analysis of Surface Waves (MASW) Method, (Figure 1), 1–16.

Park, C. B., Miller, R. D., Xia, J., & Ivanov, J. (2004). MASW An Easy Seismic Method to Map Shear-Velocity (Vs) of the Ground*.

Park, C. B., Survey, K. G., & West, C. (1995). Characterization of Geotechnical Sites by Multi-Channel Analysis of Surface Waves (MCASW).

Penumadu, D., & Park, C. B. (2005). Multichannel Analysis of Surface Wave (MASW) Method for Geotechnical Site Characterization. *Earthquake Engineering and Soil Dynamics*, 1–10. https://doi.org/10.1061/40779(158)3.

Philip Kearey, B. M. and I. H. (2002). *An Introduction to Geophysical Exploration*. https://doi.org/10.1128/AAC.03728-14.

Singh, Y. (2013). Electrical Resistivity Measurements: a Review. *India International Journal of Modern Physics: Conference Series*, *22*, 745–756. https://doi.org/10.1142/S2010194513010970.

Thitimakorn, Rachukarn, & P. (2013). Comparison of Two Geophysical Methods to Investigate Sand and Gravel Deposits , a, *7*(7), 761–767.

USDA. (2001). *Soil Survey of Will County*.

V. Torgashov, E. LANE SPRING CASE STUDY (2012).

Xia, J., Miller, R. D., & Park, C. B. (1999). Configuration of near surface shear wave velocity by inverting surface wave. *Proceedings of the Symposium on the Application of Geophysics to Engineering and Environmental Problems*, *99*(1885), 95–104.

Xia, J., Miller, R. D., Park, C. B., Ivanov, J., & Survey, K. G. (1999). High-frequency Rayleigh wave and its applications in near-surface geophysics High-frequency Rayleigh wave and its applications.

Zhou, W., Beck, B. F., & Adams, A. L. (2002). Effective electrode array in mapping karst hazards in electrical resistivity tomography. *Environmental Geology*, *42*(8), 922–928. https://doi.org/10.1007/s00254-002-0594-z.

VITA

Ragab Jaafar was born in 1986, in Benghazi City, Libya. In 2005 graduated from Middle School and entered University of Benghazi, Libya, and graduated from it in 2009 and received a Bachelor of Science degree in Geophysics.

He obtained practical experience in geophysical data acquisition, data processing, and data interpretation called "Geophysical field methods" during a Summer Internship in The Arabian Gulf Oil Company (AGOCO) in Libya. 2010.

In August 2014, Mr. Jaafar started the Master program in Geological Engineering (M.S.) at Missouri University of Science and Technology in Rolla, Missouri. During his Master program, he participated in a couple of applied geophysics projects that focused on imaging shallow subsurface by using the Ground Penetrating Radar, Multichannel Analysis of Surface Waves, Electrical Resistivity Tomography, and Seismic Refraction.

He has been an active member of different professional organizations including American Association of Petroleum Geologists: Student member, Society of Exploration Geophysicists and Geological Society of America: Student member.

In July 2017, he received his Master's degree in Geological Engineering from the Missouri University of Science and Technology, Rolla, United States of America.